JGR Solid Earth

RESEARCH ARTICLE
10.1029/2020JB019576

The Role of Premagmatic Rifting in Shaping a Volcanic Continental Margin: An Example From the Eastern North American Margin

G. Lang[1], U. S. ten Brink[1,2], D. R. Hutchinson[2], G. S. Mountain[3], and U. Schattner[1]

[1]Dr. Moses Strauss Department of Marine Geosciences, Charney School of Marine Sciences, University of Haifa, Haifa, Israel, [2]Woods Hole Science Center, U.S. Geological Survey, Woods Hole, MA, USA, [3]Department of Earth and Planetary Sciences, Rutgers, State University of New Jersey, Piscataway, NJ, USA

Key Points:
- Rift structure, crustal thickness, and distribution of breakup volcanism of the Eastern North American volcanic margin are presented
- Georges Bank Basin experienced substantial premagmatic thinning, whereas Baltimore Canyon Trough thinning was magma assisted
- Inherited distribution of crustal rheology determined the nature and intensity of premagmatic strain

Supporting Information:
- Supporting Information S1

Correspondence to:
G. Lang,
glang@campus.haifa.ac.il

Citation:
Lang, G., ten Brink, U. S., Hutchinson, D. R., Mountain, G. S., & Schattner, U. (2020). The role of premagmatic rifting in shaping a volcanic continental margin: An example from the Eastern North American Margin. *Journal of Geophysical Research: Solid Earth*, *125*, e2020JB019576. https://doi.org/10.1029/2020JB019576

Received 10 FEB 2020
Accepted 7 OCT 2020
Accepted article online 12 OCT 2020

Abstract Both magmatic and tectonic processes contribute to the formation of volcanic continental margins. Such margins are thought to undergo extension across a narrow zone of lithospheric thinning (~100 km). New observations based on existing and reprocessed data from the Eastern North American Margin contradict this hypothesis. With ~64,000 km of 2-D seismic data tied to 40 wells combined with published refraction, deep reflection, receiver function, and onshore drilling efforts, we quantified along-strike variations in the distribution of rift structures, magmatism, crustal thickness, and early post-rift sedimentation under the shelf of Baltimore Canyon Trough (BCT), Long Island Platform, and Georges Bank Basin (GBB). Results indicate that BCT is narrow (80–120 km) with a sharp basement hinge and few rift basins. The seaward dipping reflectors (SDR) there extend ~50 km seaward of the hinge line. In contrast, the GBB is wide (~200 km), has many syn-rift structures, and the SDR there extend ~200 km seaward of the hinge line. Early post-rift depocenters at the GBB coincide with thinner crust suggesting "uniform" thinning of the entire lithosphere. Models for the formation of volcanic margins do not explain the wide structure of the GBB. We argue that crustal thinning of the BCT was closely associated with late syn-rift magmatism, whereas the broad thinning of the GBB segment predated magmatism. Correlation of these variations to crustal terranes of different compositions suggests that the inherited rheology determined the premagmatic response of the lithosphere to extension.

1. Introduction

Deep-rooted tectonic and magmatic processes accompany the extension and breakup of continents, leading to the formation of passive continental margins. The resultant rifted margins are broadly divided into volcanic and magma-poor margins (Figure 1; e.g., Doré & Lundin, 2015; Franke, 2013; Menzies et al., 2002; Mutter et al., 1988). The structures and petrological properties of these two archetype margins are described as dichotomic. Whereas magma-poor margins usually consist of a wide zone of crustal necking, hyperextension, and exhumation of lower crust and mantle rocks (Figure 1b; e.g., Franke, 2013; Peron-Pinvidic et al., 2013; Reston, 2009), volcanic margins are often described as having narrow zones of crustal thinning (<100 km) adjacent to thick intrusive and extrusive magmatic additions (Figure 1a; e.g., Franke, 2013; Lizarralde & Holbrook, 1997; Stica et al., 2014).

The processes that thin the continental crust and mantle lithosphere giving rise in magma-poor margins were extensively modeled in recent years (e.g., Brune et al., 2014, 2017; Huismans & Beaumont, 2011, 2014; Lavier & Manatschal, 2006; Peron-Pinvidic et al., 2013; Reston, 2009; Sutra et al., 2013). The formation of volcanic margins on the other hand remains unsettled. Volcanic margins may result from heating of the upper mantle by either a plume head (White et al., 1987; White & McKenzie, 1989) or nonplume-related processes (Kelemen & Holbrook, 1995; McHone, 2000) such as continental insulation (Anderson, 1982; Brandl et al., 2013) or small-scale convection induced by sharp lithosphere necking (King & Anderson, 1998; Mutter et al., 1988). However, it is not clear whether the initial lithosphere thinning mechanisms leading to the formation of volcanic margins are distinct (e.g., Mutter et al., 1988; White & McKenzie, 1989) or are mostly similar to the mechanical rifting processes that form magma-poor margins (Eldholm et al., 2000; Guan et al., 2019). It is widely accepted that the inherited structure and composition of the pre-rift lithosphere control the deformation and thinning patterns at rifts and passive margins (e.g., Brune et al., 2017;

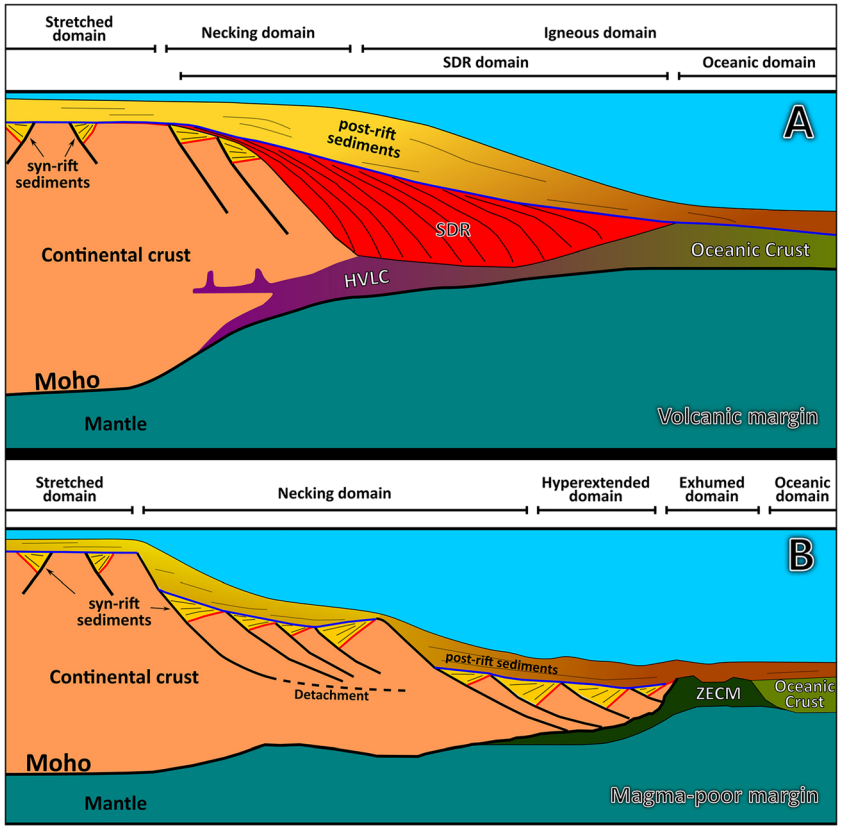

Figure 1. Schematic comparison between (a) a volcanic continental margin (modified after Doré & Lundin, 2015; Eldholm et al., 1995; Franke, 2013) and (b) a magma-poor continental margin (modified after Doré & Lundin, 2015; Franke, 2013; Peron-Pinvidic et al., 2013; Sutra et al., 2013). Abbreviations: HVLC = high-velocity lower crust; SDR = seaward dipping reflectors; ZECM = zone of exhumed continental mantle.

Manatschal et al., 2015; Misra & Mukherjee, 2015). However, less is known about the role that inheritance plays during the formation of volcanic margins, as weakening by heating and intrusions might overwhelm the inherited rheological signal.

We use an extensive set of seismic reflection and auxiliary data along the volcanic Eastern North American Margin (ENAM; Figure 2) to constrain syn-rift crustal and lithosphere thinning patterns at a margin-wide scale. We show that (a) the width of the zone of crustal thinning varies along the margin; (b) extensive (>200 km wide) crustal and lithosphere thinning predated volcanic breakup in the Georges Bank Basin (GBB) segment, contradicting some existing models for the formation of volcanic margins; (c) rifting of the ENAM can be divided into premagmatic and magmatic rifting stages; (d) the distribution, width, and nature of premagmatic thinning are controlled by the pre-rift rheology; and (e) magmatic rifting is accompanied by major strain localization and intense crustal thinning.

1.1. Crustal Structure

The most pronounced characteristic of volcanic margins is the magmatic addition related to their latest stage of formation. These include a thick (<20 km) wedge of subaerially emplaced volcanic rocks, which were imaged on seismic reflection data as oceanward/seaward dipping reflectors (SDR) (Figure 1b; Hinz, 1981; Mutter et al., 1982; Planke et al., 2000) and an intruded and/or underplated lower crust (e.g., Abdelmalak et al., 2017; Eldholm et al., 1995; Holbrook et al., 1992; Menzies et al., 2002; White et al., 1987). SDR emplacement occurs on top of seaward tilting blocks composed of intruded continental or oceanic crust (Geoffroy, 2005; Stica et al., 2014). Alternatively, they tilt as a response to flexural subsidence of gabbroic dikes that form their base (Mutter et al., 1982; Paton et al., 2017; Tian & Buck, 2019). The SDR transform seaward into an abnormally thick oceanic crust that gradually thins to typical oceanic thicknesses away

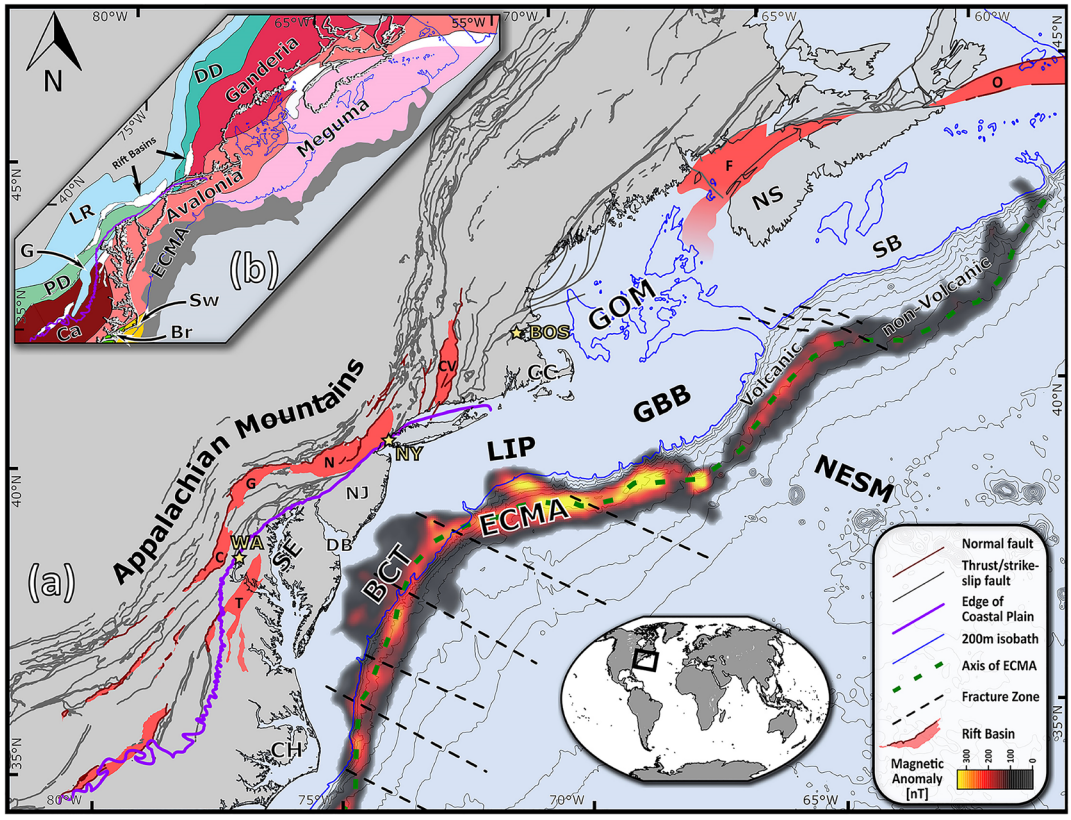

Figure 2. (a) Major geological features of eastern North America. Light gray contours are 1 km spaced bathymetry contours. East Coast magnetic anomaly (ECMA) data are after Meyer et al. (2017). Locations of early Mesozoic rift basins are marked with red shading after Klitgord et al. (1988) and Withjack et al. (2002) and references therein. Oceanic fracture zones and onshore faults (dark gray lines) are after Hibbard et al. (2006) and Klitgord et al. (1988), respectively. The transition from a volcanic to a nonvolcanic margin south of Nova Scotia is marked after Deptuck and Kendell (2017). Locations of major cities are indicated as stars. The segments of the Eastern North American Margin are BCT = Baltimore canyon trough, LIP = Long Island platform, GBB = Georges Bank basin, SB = Scotian Basin. Main rift basins: C = Culpeper; CV = Connecticut Valley; F = Fundy; G = Gettysburg; O = Orpheus; T = Taylorsville. Other abbreviations: CH = Cape Hatteras; CC = Cape Cod; DB = Delaware Bay; GOM = gulf of Maine; NESM = New England seamount chain; NJ = New Jersey; NS = Nova Scotia. b) Distribution of crustal building blocks and terranes (after Hatcher et al. (2010) , Hibbard et al. (2006, 2007) and Sheridan et al. (1993)). Br = Brunswick; Ca = Carolina; DD = Dunage domain; G = Goochland; LR = Laurentian realm; PD = Piedmont domain; Sw = Suwannee.

from the continent (Menzies et al., 2002). In most volcanic margins, the transition from an unthinned continental crust to an igneous/oceanic crust occurs over relatively short distances (50–100 km, indicated by the "Necking domain" in Figure 1a; Ebinger & Casey, 2001; Franke, 2013; Paton et al., 2017; White & McKenzie, 1989; White et al., 1987). Nevertheless, volcanic margins might exhibit wider geometries where older rifting episodes predated volcanic breakup (Guan et al., 2019). Another phenomenon often associated with volcanic margins is the emplacement of large igneous provinces shortly before or during rifting (Menzies et al., 2002; White & McKenzie, 1989; Ziegler & Cloetingh, 2004).

Magma-poor margins seldom include the magmatic components described above. However, they are associated with other unique characteristics such as hyperextended crust (<10 km thick and composed of brittle hydrated crust), detachment faults, and exhumed mantle rocks (Figure 1b; Lavier & Manatschal, 2006; Manatschal, 2004; Sibuet et al., 1987). The along-dip extent of the thinned continental crust is usually wider than that found in volcanic margins and may reach up to 350 km (e.g., profile SMART 2 in Nova Scotia which appears at Wu et al., 2006).

1.2. Modes of Rifting

The sequence of events leading to the formation of volcanic and magma-poor margins is also different. In a broad sense, the formation of magma-poor margins involves the breakup of the continental crust before the

breakup of the mantle lithosphere (e.g., Reston, 2009), whereas rifting of volcanic margins is thought to involve the breakup of the mantle lithosphere before or concomitantly with the total breaking of the crust (Franke, 2013). Magma-poor margins often experience polyphase rifting and relatively low strain rates during their formation (<15 mm/year half extension rate, Lundin et al., 2014 and references therein). This slow and protracted rifting promotes a broad zone of crustal thinning (Reston, 2009, and references therein). The formation of volcanic margins, on the other hand, is associated with high strain rates (25–30 mm/year half extension, Hopper et al., 2003; Schreckenberger et al., 2002), increasing weakening of the lithosphere and strain localization toward the rift axis (Buck, 2004, 2006).

A widely accepted model for the formation of the igneous material that characterizes volcanic margins considers rifting over a mantle hotter than normal by at least 150°C (White & McKenzie, 1989). The increased mantle temperature is attributed to the presence of a mantle plume under a continental rift (White et al., 1987; White & McKenzie, 1989) or to upper mantle convection (e.g., Anderson et al., 1992; Kelemen & Holbrook, 1995). This model treats the co-occurrence of rifting and mantle heating as incidental, yet it requires both. Once the lithosphere has been thinned by a factor of ~5, it breaks, allowing melt to migrate to the surface. Part of the melt might not reach the surface and accumulate at the base of the crust (White et al., 1987; White & McKenzie, 1989).

Other models suggest convective partial melting under rifts as an explanation for melt production during the formation of volcanic margins (Mutter et al., 1988). These models do not necessarily require increased temperatures to produce melts. Rather, they require rapid and localized lithospheric thinning that promotes a sharp relief at the lithosphere-asthenosphere boundary under the rift (Mutter et al., 1988; Van Wijk et al., 2001). The asthenospheric material that rises into the region of thinned lithosphere is hotter than its surroundings. Lateral temperature and density differences drive small-scale convection under the rift, bringing more hot asthenosphere from below and increasing the generation of melts. (Simon et al., 2009; Van Wijk et al., 2001).

Although the convective partial melting models outline an inverse cause-and-effect scenario to the one depicted by rifting over hotter-than-normal mantle models, both types of models predict margins with narrow zones of crustal and lithospheric thinning (Figure 1a). The sharp lithosphere-asthenosphere boundary, a requisite for convective partial melting models, implies that the thinning must be limited to a narrow zone (~100 km; Mutter et al., 1988). According to White and McKenzie (1989), the presence of hot asthenosphere under a rift weakens the lithosphere and promotes strain localization toward the rift axis. If breakup is achieved, strain localization leads to the formation of a narrow margin. Later works further proposed that large quantities of magma generated during rifting over a heated mantle would intrude and heat the lithosphere, reducing the tensile stress required to split it (Buck, 2004, 2006). This "magma-assisted rifting" mechanism was used to explain observations of minor crustal thinning coincident with large amounts of breakup magmatism at the east Africa rift system (Buck, 2006; Kendall et al., 2005). Recently, Geoffroy et al. (2015) proposed that two conjugate syn-volcanic crustal-scale detachment faults accommodate most of the crustal thinning at volcanic margins. The subsiding hanging walls of these faults accommodate extrusive flows (SDR), forming a relatively sharp hinge between the untinned and igneous crust (Stica et al., 2014).

Despite the considerable amount of research on the evolution of volcanic margins, the nature of crustal deformation, the processes that involve the premagmatic extension and the implication these have for the post-rift evolution of such margins remain unclear. To investigate these unresolved issues, the current study examines the ENAM. The ENAM is chosen due to its relatively continuous and well-constrained rifting phase and the availability of recently released seismic and borehole data (Triezenberg et al., 2016). These data, coupled with the availability of modern interpretation and visualization software, allow the documentation of along-margin variations in greater detail than was previously possible. We examine the syn-rift and post-rift evolution of the Baltimore Canyon Trough (BCT) and GBB (Figure 2) and specifically the extent and geometry of their crustal thinning and distribution of SDR.

2. The Eastern North American Volcanic Margin

The geology of the ENAM records two full Wilson cycles. The last cycle included the closure of the Iapetus and Rheic Oceans (e.g., van Staal et al., 2009) and the formation of the supercontinent Pangea between 420 and 270 Ma (Thomas, 2006, and references therein). Late Triassic to Early Jurassic rifting of Pangea

(e.g., Olsen, 1997; Withjack et al., 2012) was accompanied by the formation of a series of asymmetric rift basins (i.e., half-grabens, Figure 2). The North American remnant of this rift system is bounded by the Appalachian Mountains to the NW and the continent-ocean boundary to the SE (roughly at the present-day continental slope, Figure 2; e.g., Leleu et al., 2016; Withjack et al., 2012). The basins accumulated a well-documented Triassic-early Jurassic syn-rift sequence (e.g., Leleu & Hartley, 2010; Olsen, 1997; Schlische, 1992). The syn-rift sequence records the emplacement of an intense magmatic event that occurred at ~200 Ma known as the Central Atlantic Magmatic Province (CAMP; e.g., Hames et al., 2000; Marzoli et al., 1999, 2011, 2018; Nomade et al., 2007; Olsen, 1999; Olsen et al., 2003; Whiteside et al., 2007). Rift basin subsidence in central North America ended soon after the CAMP magmatism (Withjack et al., 2012). Cessation of rifting was attributed to lithospheric breakup associated with the opening of the Atlantic Ocean. Estimates for the age of breakup range between 175 Ma (Klitgord & Schouten, 1986) and 190 Ma (Labails et al., 2010; Sahabi et al., 2004; Sibuet et al., 2012) and 200 Ma (Schettino & Turco, 2009). It was proposed that breakup was diachronous, starting at ~200 Ma in southern North America, advancing to central North America at 195–175 Ma (Withjack et al., 1998, 2012). Shuck et al. (2019) suggest that accretion of protooceanic crust occurred over an unbroken lithosphere starting at ~200 Ma. They claim that full lithospheric breakup was achieved at 175 Ma when normal seafloor spreading began. By the end of the rifting phase, post-rift thermal subsidence dominated the vertical motions on the continental margin (e.g., Sawyer, 1985; Steckler & Watts, 1978; Swift et al., 1987).

The discovery of magmatic material, that was accreted during the latest stages of rifting and earliest seafloor spreading, led to the recognition of the volcanic nature of the ENAM (Austin et al., 1990; Holbrook et al., 1992, 1994; Holbrook & Kelemen, 1993; Keen & Potter, 1995; Kelemen & Holbrook, 1995; LASE, 1986; Lizarralde & Holbrook, 1997; Talwani et al., 1995; Tréhu et al., 1989). Holbrook and Kelemen (1993) correlated intrusive and extrusive bodies, recognized on several wide-angle seismic profiles along the margin, to a margin-parallel positive magnetic anomaly known as the East Coast Magnetic Anomaly (ECMA, Figure 2). Hence, magmatism was regional, spanning over ~2,000 km from the Blake Plateau Basin to offshore southern Nova Scotia. This East Coast Margin Igneous Province (ECMIP) is comprised of an SDR wedge inferred to be extrusive basalt above its intrusive counterpart in the form of a high-velocity lower crust (Vp = ~7.5 km/s). Wide-angle seismic data reveal that the continental crust thins rapidly seaward toward a point of convergence between the high-velocity lower crust and SDR. Seaward of this point, the crust is entirely igneous (LASE, 1986; Tréhu et al., 1989). At the BCT, the maximum thickness of the igneous crust is 13–24 km (Talwani et al., 1995).

Models for the emplacement of ECMIP favor minor prebreakup lithospheric thinning over an abnormally hot asthenosphere. A mantle plume was suggested as the source of excess heat (White & McKenzie, 1989). The plume was probably situated at the southern part of the rift system, near Florida (e.g., Ruiz-Martínez et al., 2012; Wilson, 1997). Other proposed heating mechanisms include continental insulation (e.g., Hole, 2015), edge-driven convection (McHone, 2000), and slab delamination processes (Whalen et al., 2015). Kelemen and Holbrook (1995) suggested that the magma originated in partial melting of hotter-than-normal mantle (>1500°C) under high pressure (>4 GPa). They proposed a scenario in which the lithosphere acted as a thick lid due to a minor amount of thinning until the final stages of rifting. Reprocessing of the data set used by Kelemen and Holbrook (1995) led Talwani and Abreu (2000) to suggest that a 30 km thick continental crust juxtaposes an igneous crust of comparable thickness at the BCT. They inferred that crustal thinning was minimal and required high mantle temperatures. Farther south, under the Carolina Trough (Figure 2), a similar crustal structure was observed and may also imply minor thinning prior to breakup (Tréhu et al., 1989). Since ECMIP rocks have not been sampled offshore, the exact age of the ECMIP and its relation to the CAMP are unresolved issues. Age estimates for the ECMIP are 172–179 Ma (Benson, 2003), 175 Ma (Klitgord & Schouten, 1986) and 190 Ma (Labails et al., 2010; Sibuet et al., 2012). Recently, Davis et al. (2018) suggested that ECMIP is the offshore continuation of CAMP and that its emplacement took between 6 to 31 Myr, starting at ~201 Ma and ending between 195 and 170 Ma.

Although the ENAM is volcanic from the Blake Plateau Basin in the south to the Scotian Basin in the north, previous studies have noticed that it is segmented. The segmentation is reflected in the location of the hinge zone, geometry of the rift basins, characteristics of the post-rift unconformity, post-rift sedimentation, elastic thickness of the lithosphere, and details of gravity and magnetic anomalies along the strike of the margin (Behn & Lin, 2000; Klitgord et al., 1988; Wyer & Watts, 2006). When suggesting an explanation for the

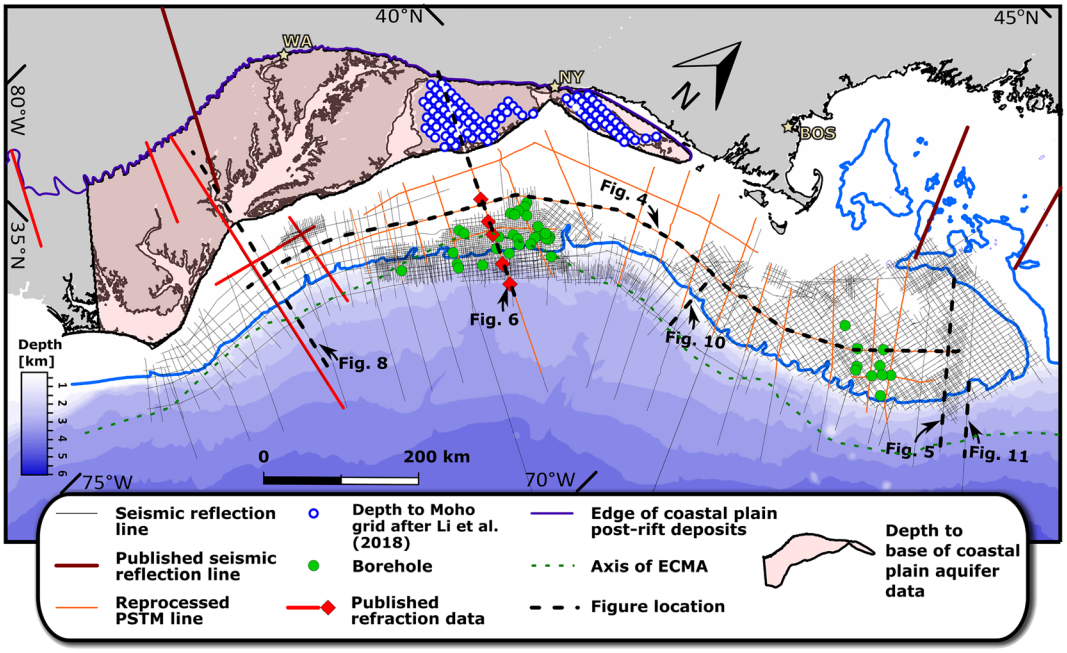

Figure 3. Distribution of data used superimposed on bathymetry. Black and blue lines mark the locations of the present-day shoreline and 200 m isobath, respectively. Red diamonds are locations of LASE (1986) expanded spread profile data. Onshore depth to base of coastal plain aquifer is from Pope et al. (2016). Bathymetry data are from Andrews et al. (2013). BOS = Boston; NY = New York; WA = Washington.

along-strike heterogeneity of the ENAM, some of the cited studies emphasize allogenic factors such as sediment supply (Poag & Sevon, 1989), whereas others suggested autogenic controls such as rift-related variations in lithospheric strength (Wyer & Watts, 2006). Works predating the recognition of the margin as volcanic explained the along-strike variations using rifting models that are more suitable for magma-poor settings (e.g., upper plate vs. lower plate, Klitgord et al., 1988). The current study aims at explaining these variations in the context of a volcanic margin.

3. Data and Methods

We used a comprehensive set of seismic reflection data acquired on the continental shelf and slope from the United States-Canada border to Cape Hatteras (Figure 3 and Table S1 in the supporting information). The 64,000 km of 2-D seismic profiles was acquired as 4,147 lines using a variety of acquisition parameters during 23 cruises for industry and research from the 1970s to the 1990s (e.g., Benson & Doyle, 1988; Klitgord et al., 1988, 1994; Poag, 1991; Poag & Sevon, 1989; Schlee & Fritsch, 1982). The industry data are archived at the U.S. Geological Survey (USGS) National Archive of Marine Seismic Surveys (Triezenberg et al., 2016). Approximately 4,000 km of the seismic data was reprocessed as part of an offshore CO_2 sequestration evaluation project (Cumming et al., 2017; Fortin et al., 2018).

Forty offshore wells were incorporated (Figure 3). Well data include paleontological reports, check-shot records, and geophysical well logs such as sonic and density logs (Table S3). The data were scanned and digitized as part of the offshore CO_2 sequestration project (Cumming et al., 2017).

A compilation of published results of wide-angle seismic, deep reflection seismic, and receiver function data helped constrain crustal thicknesses (Figure 3 and Table S2 in the supporting information). As part of this compilation, depth domain data were converted into two-way travel time (TWT) based on refraction results (Figure 3 and Table S2 in the supporting information). The domain conversion was done from depth to TWT and not vice versa for three reasons. First, most of the data used are in the TWT domain. Second, depth domain data are restricted to areas of thin or no sediment cover. This makes their domain conversion function more straightforward compared with most of the TWT data which are found in areas with thicker

(>3 km) sediment cover. Third, the TWT domain allows the interpretation of crustal boundaries and large thickness changes using few assumptions and without having to rely on the choice of conversion velocities. For onshore depth data, an average of 6.3 km/s conversion velocity was used for the continental crust (Lizarralde & Holbrook, 1997; Pratt et al., 1988). A depth to Moho grid by Li et al. (2018) was used for constraining Moho onshore the northern BCT. The grid is the outcome of interpolation of multiple receiver function stations. The digital version of the grid used here (V. Levin, written Comm., 2019) extends farther south with respect to the grid presented by Li et al. (2018) and covers the entire New Jersey state area. For offshore data at the northern BCT, lithological boundaries (Figure 5 in LASE, 1986) were digitized on five Expanded Spread Profiles following the interpretation of Talwani et al. (1995). Since no refraction data cross the GBB and LIP, constraints on the crustal structure in these areas rely on reflection data alone.

Magnetic anomaly data were used to constrain the ECMA and infer on its relation to the margin structure and especially the SDR. The EMAG2v3 (Version 3) global magnetic anomaly grid used here incorporates satellite, ship, and airborne magnetic measurements and features a 2 arc-minute resolution (Meyer et al., 2017).

Depth to the base of the post-rift (BPR) beneath the coastal plain was constrained using a digital elevation map by Pope et al. (2016). The map illustrates the structure of the base of the U.S. North Atlantic coastal plain aquifer from New York in the north to the southern part of North Carolina in the south (Figure 3). The coastal plain aquifer is composed of the post-rift sequence. Hence, the base of the aquifer separates pre-rift basement rocks and syn-rift strata below from the overlying post-rift sequence. The mapping of the base of the aquifer (post-rift) by Pope et al. (2016) relies on a regional amalgamation of results of previous studies, which defined the aquifer based on well-log data. The Pope et al. (2016) digital elevation map was only used onshore and was smoothed using a 1 km by 1 km window. The map was converted to TWT using an average velocity of 2.5 km/s based on the average velocity observed for the equivalent depth interval at the wells located on the outer shelf (e.g., COST B-2, Smith et al., 1976).

3.1. Seismic Interpretation

Four horizons/horizon packages have been mapped to identify and understand the rifting, basement, and crustal geometries: top of basement, SDR, the Moho, and BPR. An additional six post-rift horizons have been mapped and will be reported elsewhere.

3.1.1. Top Basement

Since only one well, the COST G-1 well, penetrated pre-rift basement rocks in the study area, the main input for mapping the top basement is seismic reflection data. On seismic sections, the sediment-basement interface usually appears as a high-amplitude reflector that separates continuous sedimentary reflectors above from discontinuous, chaotic reflectors below (Figures 4–6). In several locations (e.g., the Long Island Platform and some rift basins at the GBB) along the margin, the upper part of the basement appears to be reflective as well. This phenomenon may be attributed to pre-rift sediments or metasediments or to “ghost” artifacts, and it sometimes obscures picking the top of basement. Where those upper crust reflectors appear, the interpretation follows a high-amplitude reflector that is onlapped by post-rift reflectors (Figure 4). Inside rift basins, where dipping, divergent reflectors mark syn-rift strata (e.g., Klitgord et al., 1988); the top of basement is regarded as the base of the divergent wedge (red line, Figures 4b and 5b). At the deepest parts of GBB and BCT the interpretation of top basement is ambiguous. To reduce the uncertainty in picking top basement at these areas, the results of published refraction surveys were used to guide the interpretation of reflection data (Figures 3, 4, and 6). The absence of deep refraction data at the GBB makes the interpretation of its deepest part (>5 s TWT) less certain.

3.1.2. Seaward Dipping Reflectors

Multichannel seismic reflection, together with published refraction data, was also used to map the extent of SDR along the continental shelf, slope, and rise. The SDR were mapped based on their reflection geometry following the definition of Mutter et al. (1982). In addition, published wide-angle seismic data were used to constrain the interpretation and to increase data coverage. The TWT values of the top of the SDR in northern BCT were repicked on published five expanded spread profile velocities (LASE, 1986). The top of the SDR was assigned to an increase in *P* wave velocity from ~5.7 to ~6.1 km/s. The corresponding TWT values were then placed on the USGS Profile 25 at each expanded spread profile location and compared to the seismic reflection data. Previous interpretations of the three EDGE profiles (Sheridan et al., 1993) were digitized

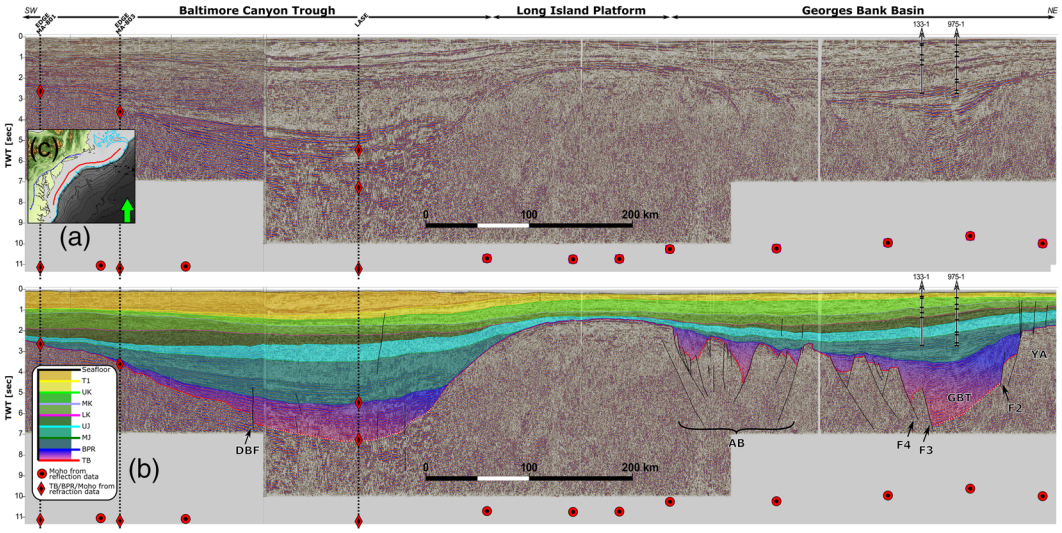

Figure 4. (a) Composite multichannel seismic reflection section of prestack time migrated USGS profile 12 and industry data, along the strike of the ENAM. (b) Interpretation of a. inset shows stratigraphy color code (see Table S1 for the ages of the horizons). Red circles mark locations of Moho reflectors as they appear on crossing dip-oriented reflection profiles. Red rhombuses are locations of the Moho, top basement, and base post-rift horizons based on crossing seismic refraction profiles, which are indicated by vertical dashed lines. Projections of two wells, located less than 2 km NW of the profile, are shown in the Georges Bank basin. (c) Map showing the profile location. AB = Atlantis Basin; DBF = Delaware Bay fault; GBT = Georges Bank trough; YA = Yarmouth arch.

for mapping the top of the SDR at the southern BCT. The top SDR horizon, as recognized on both reflection and refraction data, was then traced regionally using seismic reflection profiles.

3.1.3. Moho

The base of the seismic crust (Moho) was mapped according to both deep seismic reflection and published refraction data. Moho reflection were interpreted as deep (9–12 s), mostly continuous, low-frequency reflectors at the base of a reflective interval that can be distinguished from an underlying transparent zone (pink line, Figure 5). These reflectors appear only on data collected by the USGS. The interpretation of these

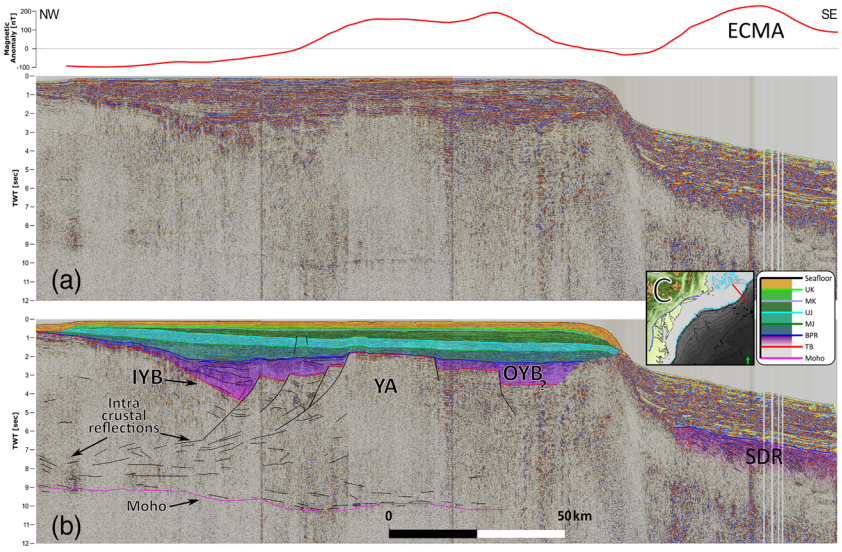

Figure 5. (a) USGS multichannel seismic reflection profile 18 across the northern GBB continental shelf, slope, and rise. (b) Interpreted section. Inset shows stratigraphy color code (see Table S1 for the ages of the horizons). (c) Map showing the profile location. Magnetic anomaly profile is shown across the top of the section a. ECMA = East Coast magnetic anomaly; IYB = inner Yarmouth Basin; OYB = outer Yarmouth Basin; SDR = seaward dipping reflectors; YA = Yarmouth arch.

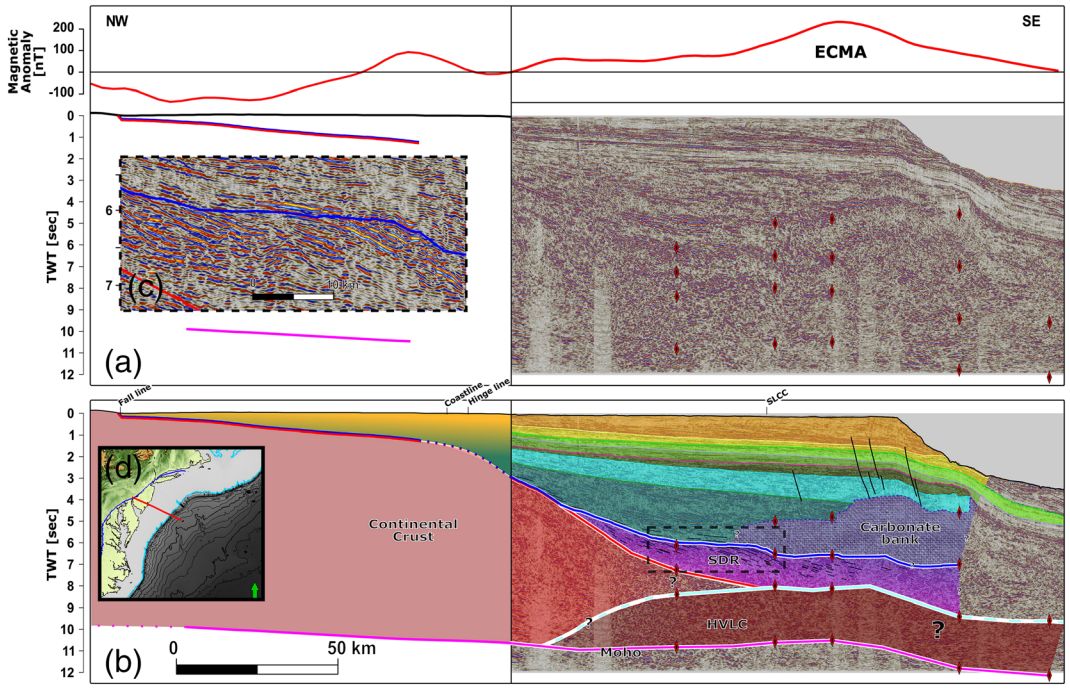

Figure 6. (a) Dip-oriented section across the northern Baltimore canyon trough composed of reprocessed, prestack time-migrated USGS multichannel reflection profile 25 offshore and base of coastal plain aquifer digital elevation map, and results of receiver function analysis used to mark the BPR and Moho onshore. (b) Interpreted section. Red rhombuses mark constraints of the locations of the Moho, high-velocity lower crust (Vp > 7.1 km/s), top basement, seaward dipping reflectors package, and top carbonate bank based on reinterpretation of wide-angle seismic results (LASE, 1986). Positions of the base post-rift, the Moho west of the hinge line, and the seaward limit of continental crust are after Li et al. (2018), Pope et al. (2016), and Talwani et al. (1995), respectively. See Figure 3 for description of the stratigraphy. Dashed rectangle marks location of C. (c) Uninterpreted, vertically exaggerated magnification of the part in (a) that shows SDR. (d) Map showing the section location. ECMA = East Coast magnetic anomaly; HVLC = high-velocity lower crust; SDR = seaward dipping reflectors; SLCC = seaward limit of continental crust.

reflectors to be the Moho agrees with previous interpretations of the same data at the Long Island Platform (Hutchinson et al., 1985, 1986), the Gulf of Maine (Hutchinson et al., 1987, 1988), and other seismic data in the ENAM (Keen et al., 1991; LASE, 1986; Lizarralde & Holbrook, 1997; Sheridan et al., 1993). Previous interpretations of the Moho underneath the continental shelf were extended by using two seismic attributes with seismic interpretation: structural smoothing to increase reflector continuity and time-varying gain.

3.1.4. Base Post-rift

The base post-rift (BPR) horizon is a combination of three stratigraphic tops: the top of SDR, the top of syn-rift strata, and the top of basement. Where rift basins are present, the BPR is interpreted as an erosional surface that separates the divergent syn-rift strata from onlapping and sagging post-rift strata (Figures 4 and 5). Where SDR are apparent, the BPR is placed at the top of the seaward dipping package (Figures 5 and 6). In places where neither SDR nor syn-rift strata appear, the BPR coincides with top basement. The time span of the hiatus across the BPR unconformity should generally increase landward. Though diachronous, the BPR unconformity should correspond to the time interval during which rifting had ceased and post-rift subsidence commenced seaward of the hinge line. Early estimates for rift cessation point to early Hettangian age (201 Ma; Walker et al., 2018), while the latest estimates for initiation of seafloor spreading are of early Aalenian (174 Ma; Walker et al., 2018; for further discussion see Withjack et al., 2012).

3.1.5. Post-rift Horizons

Interpretation of post-rift horizons follows standard seismic interpretation procedures of sedimentary units (e.g., Mitchum et al., 1977; Vail et al., 1977). Available wells were tied to sequence bounding surfaces to constrain the ages of the interpreted horizons (For a detailed description of seismic well tie procedures and paleontological data see Table S3). In total, six post-rift horizons were mapped along the margin (Figure 4 and Table 1). Paleontological reports are in general agreement regarding the ages of Cretaceous and

Table 1
Seismic Horizons and Their Corresponding Ages

Horizon	Geological period	Age (Ma)[a]
T1	Top Oligocene	23
UK	Top Cretaceous	66
MK	Middle Cenomanian	~97
LK	Top Barremian	126
UJ	Top Tithonian	145
MJ	Top Callovian (?)	164?
BPR	Hettangian (?) to early Aalenian (?)	201–174
Top basement	Paleozoic	>252
Moho	NA	

[a]Walker et al. (2018).

younger strata. Age determination for the Cretaceous sequences follows Jordan (2019), Miller et al. (2018), and Schmelz et al. (2019). There is, however, no consensus regarding the preCretaceous chronostratigraphy (For further discussion see Cousminer & Steinkraus, 1988; Poag, 1991; Poag & Valentine, 1988). The Jurassic chronostratigraphy presented here follows Poag and colleagues' interpretations (Poag, 1991; Poppe et al., 1992a, 1992b). No rocks older than Kimmeridgian were penetrated in the BCT. Thus, the age assignment of the deeper MJ horizon at the BCT follows Poag (1985), which estimated it to be Top Callovian.

4. Interpretation

4.1. Top Basement and Basement Faults

The following paragraphs describe the structure of the top basement surface and the rift basins found in the research area. Some of the rift basins were previously described (e.g., Hutchinson et al., 1985; Hutchinson & Klitgord, 1988; Klitgord et al., 1982). However, the tight grid (<7 km line spacing at the GBB) used here uncovers details that were previously concealed. It provides accurate estimates of the extent, orientation, and lateral terminations of previously recognized rift basins and the detection of new basins not identified in earlier surveys.

4.1.1. Georges Bank Basin

The top basement at the GBB has the highest density of faults of all the margin segments examined in this study (Figure 7). The faults accommodate normal displacement and form a complex array of rift basins that generally deepen toward the shelf edge. Two main fault orientations appear: NNE-SSW (AB, FB, IYB, and OYB in Figure 7) and ENE-WSW (PB, F2 in Figure 7). Smaller, secondary faults inside the Atlantis Basin are subparallel to the ENE trend. Both the existence ENE-WSW direction and secondary faults are presented here for the first time.

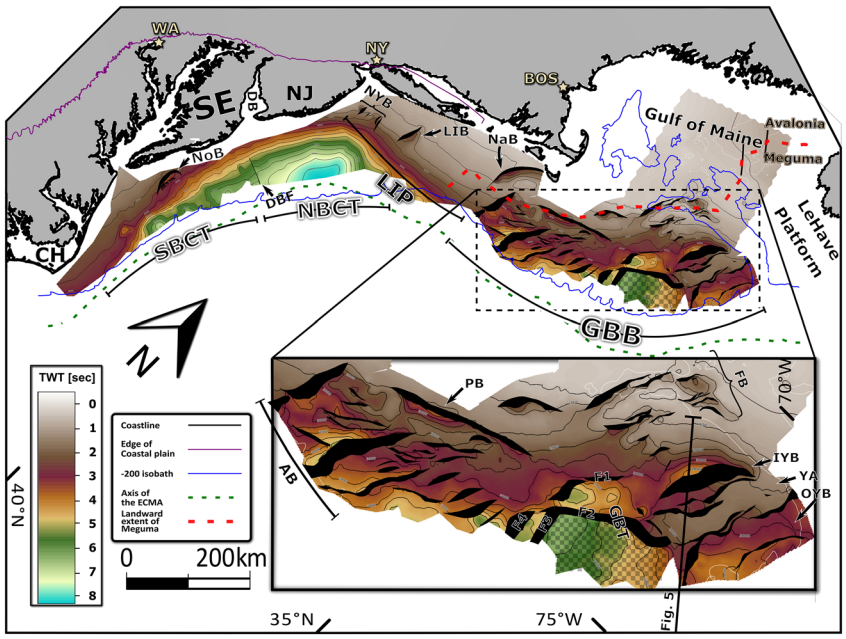

Figure 7. Structural map of top basement (in two way travel time) based on interpretations of seismic reflection and published results of seismic refraction data. Black patches mark fault heaves. Cross-hatched pattern at the GBT represents an area where interpretation is less certain. AB = Atlantis Basin; BOS = Boston; DB = Delaware Bay; DBF = Delaware Bay fault; FB = Franklin Basin; GBB = Georges Bank basin; GBT = Georges Bank trough; IYB = inner Yarmouth Basin; LIB = Long Island Basin; LIP = Long Island platform; NaB = Nantucket Basin; NBCT = northern Baltimore trough; NoB = Norfolk Basin; NY = New York; NYB = New York Bight Basin; OYB = outer Yarmouth Basin; PB = Poag Basin; SBCT = southern Baltimore canyon trough; WA = Washington; YA = Yarmouth arch.

The basement faults at the GBB dip both landward and seaward forming horsts, grabens, and half-grabens. The Atlantis Basin is composed of three main NNE striking normal faults (Figures 4 and 7). The two faults that bound the basin dip toward each other, forming a full graben with two fault-bounded highs/horsts. On a cross section, the faults appear listric with a maximum displacement of ~2 s (Figure 4). They can be traced to travel times of 5–6.5 s. The southern ending of the Atlantis Basin is unclear on the seismic data: The three main faults either terminate abruptly toward the present-day shelf edge or continue under the continental slope where data are ambiguous. A newly identified basin, the Poag Basin, bounds the northern extent of the Atlantis Basin (Figure 7). It is a 130 km long half-graben with a SW dipping listric border fault that is seismically visible to travel times of 5.5 s. North of the Poag Basin, the Franklin Basin is the shallowest basin under the GBB (Figure 7). On its western side it is bound by three en echelon normal listric faults that dip ESE and penetrate to a maximum travel time of 5.5 s. The maximum vertical displacement on the main faults is ~1.5 s. Antithetic and synthetic faults of smaller displacement are mappable to the east of the main faults.

The deepest part of the GBB, the Georges Bank Trough, is located east of the Poag and Atlantis Basins. Two normal faults bound the Georges Bank Trough to the north and west (F1 and F4 in Figure 7), whereas the Yarmouth Arch bounds it to the east. Although seismic penetration does not provide clear determination of its maximum travel time, the data provide information about its fault orientations, surface dips, and general geometry. It consists of two fault-bounded steps (the bounding faults are marked F1 and F2 in Figure 7). Both steps plunge to the SE toward N-S faults that bound the trough to the SW (F3 and F4 in Figures 4 and 7).

The area east of the Franklin Basin and north of the Georges Bank Trough diverts from the general seaward deepening trend of the margin. There, two rift basins, the Inner and Outer Yarmouth Basins are separated by a prominent basement horst—the Yarmouth Arch. The Inner Yarmouth Basin is a half-graben 50 km wide by 90 km long that extents to travel times greater than 4 s (Figures 5 and 7). The basin and faults that bound it to the east strike NNE-SSW and gradually terminate toward the LeHave Platform (Figure 7). A convergent transfer zone, where two opposing normal faults dip toward each other, separates the Inner Yarmouth Basin from the Georges Bank Trough. The dip of the eastern border faults of the Inner Yarmouth Basin is WNW making the Yarmouth Arch the footwall of this fault system. The fault system forms two to four tilted blocks between the Yarmouth Arch and the Inner Yarmouth Basin (Figures 5 and 7). Cumulative vertical displacement of the Inner Yarmouth Basin fault system reaches ~3 s. Assuming no erosion of the footwall and seismic velocity of 5 km/s for the syn-rift section, that is equivalent to more than 7 km. The cumulative heave of this fault system reaches ~18 km. On a section view, these faults appear listric (Figure 5). In their shallowest part, their inclination is 40° to 30°. The inclination decreases as they penetrate ~3.5 s into the crust.

The Inner Yarmouth Basin and its bordering fault system comprise the upper crustal manifestation of a possible crustal-scale shear zone. Figure 5 illustrates a zone of reflective lower crust <2 s above the Moho. Above this zone, at the northwestern part of the section, is a series of reflectors that mildly (<13°) dip landward. These reflectors are traceable over ~80 km, shallowing to the southeast. In the upper continental crust, these reflectors coincide with the fault system that forms the Inner Yarmouth Basin. Following the interpretation of similar observations at other rifts and continental margins (e.g., Clerc et al., 2015, 2018; Fazlikhani et al., 2017; Phillips et al., 2016; Reston et al., 1996), these inner crustal reflectors may indicate detachment faulting, crustal shearing, and ductile deformation of the crust.

The Yarmouth Arch is an ~120 km long, 30 km wide, NNE-SSW trending elongated horst found east of the Inner Yarmouth Basin. Steep, east dipping faults bound the arch to the east and separate it from the Outer Yarmouth Basin. An E-W fault, oblique to the Yarmouth Arch, marks its southern termination and separates it from the Georges Bank Trough. The structure of the southeastern corner of the arch is not well constrained by the available data. However, the trend of neighboring areas to the south and east suggests that an elevated branch of the arch may extend SE, toward the shelf edge. The Outer Yarmouth Basin is composed of two subbasins separated by an east dipping fault. Overall, the entire ~200 km wide GBB, from the western Franklin Basin to the shelf edge, represents a zone of deformed and faulted basement.

4.1.2. Long Island Platform

The top basement in the Long Island Platform is the shallowest of the three margin segments (Figures 4 and 7). It descends from near sea-surface elevation at the shoreline to about 5 s under the continental slope along a convex trajectory (Figure 7). The seismic data reveal three known rift structures: Nantucket Basin,

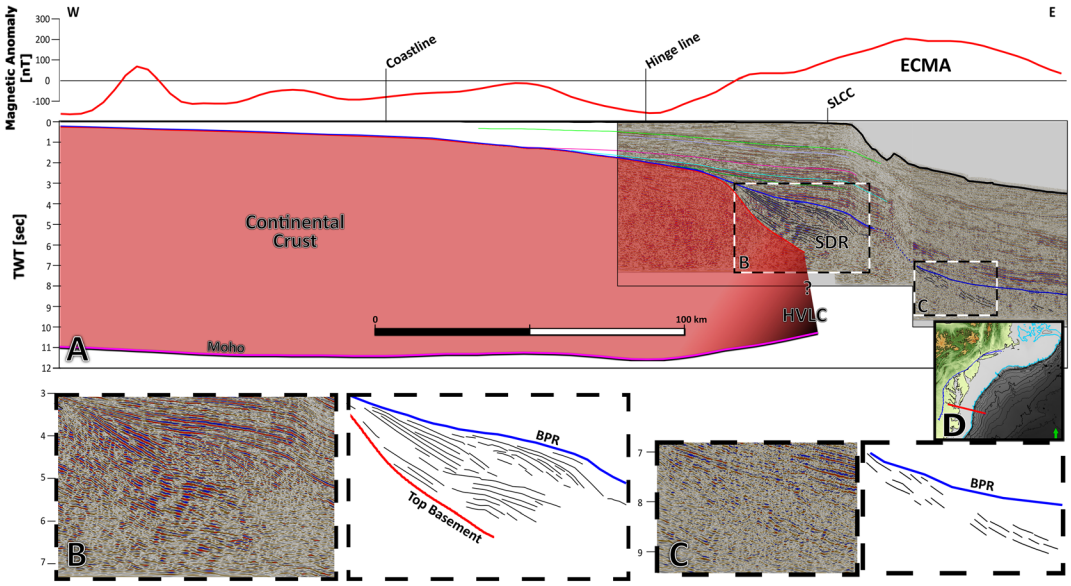

Figure 8. (a) Dip-oriented section across the southern Baltimore canyon trough coastal plain to continental rise based on MA-032 time-migrated multichannel reflection profile. Magnetic anomaly profile is shown across the top of the section. Position of the base post-rift west of the coastline is after Pope et al. (2016). Position of the Moho, top basement under the SDR, seaward limit of continental crust, and the presence of high-velocity lower crust are interpolated based on adjacent (~13 km) refraction data (Lizarralde & Holbrook, 1997; Sheridan et al., 1993; Talwani et al., 1995). Dashed rectangles mark locations of B and C. (b, c) Uninterpreted and interpretation of magnifications of the parts in (a) that show SDR. Note the overlap between the positive East Coast magnetic anomaly and the distribution of seaward dipping reflectors. (d) Map showing the profile location. See Figure 3 for description of the stratigraphy. ECMA = East Coast magnetic anomaly; HVLC = high-velocity lower crust; SDR = seaward dipping reflectors.

Long Island Basin, and New York Bight Basin (Figure 7). Nantucket Basin is located in the eastern part of Long Island Platform, NW of Atlantis Basin. It is interpreted here as an arcuate half-graben with a down to the SE boundary fault. Reaching a maximum of ~3 s TWT, it is the deepest rift basin at the Long Island Platform. At the center of Long Island Platform is the Long Island Basin. Its border fault dips toward the ESE, down throwing its hanging wall to more than 2 s. The New York Bight Basin in the western Long Island Platform is composed of five identified faults. Due to the sparsity of data in this area, its faults' orientations are not well constrained, and the interpreted dips shown in Figure 7 are apparent dips. Nevertheless, the easternmost fault of the basin was identified on two profiles as having a westward dip. Thus, the other faults of the New York Bight Basin were assigned with a similar westward dip.

4.1.3. Baltimore Canyon Trough

Offshore New Jersey, the top basement reaches more than 8 s TWT (Figures 6 and 7). Reflection data do not allow identification of a single top basement reflector or a seismic facies boundary in these deep basin areas (Figure 6). Hence, interpretation relies mostly on published refraction control points (LASE, 1986) that are tied to reflection profiles. In areas shallower than ~6 s, the top basement is identifiable on reflection data as well. In map view, the BCT has an asymmetric arcuate shape. To the north, the top basement plunges steeply southward from 1.5 s under the western Long Island Platform to 8 s over less than a 100 km. Farther SW, offshore New Jersey, the top basement dips southeastward with the same amount of deepening occurring over ~150 km. SW of New Jersey and offshore Delaware Bay, the top basement deepens to about 6 s on an ESE trajectory. At the southern BCT the top basement dips mostly to the east. There, a sharp hinge separates a shallow (<3 s), gentle top basement surface under the inner shelf from the deeper part under the outer shelf (Figures 7 and 8).

Few faults involving basement were identified at the BCT. The sparsity of faults in the deepest part, over 6 s, may be attributed to poor seismic resolution. A near-vertical, down-to-the-north, fault (Named here the Delaware Bay Fault, Figures 4 and 7) separates the deep northern BCT from the shallower southern BCT. The fault has an E-W strike and a maximum vertical displacement of ~0.5 s. A similar fault might be

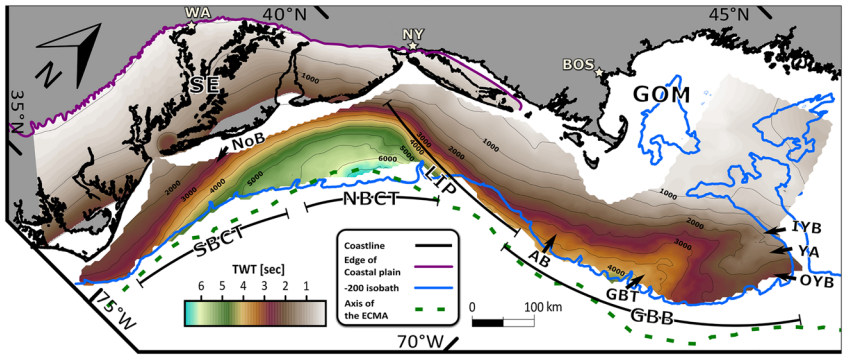

Figure 9. Two-way travel time structural map of the base post-rift. Abbreviations of names of structures underlying the BPR: AB = Atlantis Basin; GBT = Georges Bank trough; IYB = inner Yarmouth Basin; NoB = Norfolk Basin; OYB = outer Yarmouth Basin; YA = Yarmouth arch. Other abbreviations: BOS = Boston; GBB = Georges Bank basin; GOM = gulf of Maine; NBCT = northern Baltimore canyon trough; NY = New York; SBCT = southern Baltimore canyon trough; SE = Salisbury embayment; WA = Washington.

present at the opposing northern flank of the northern BCT (Figure 4), although data sparsity does not allow it to be clearly identified and mapped.

Only one rift basin can be identified at the BCT in the offshore seismic grid, the Norfolk Basin, which is located under the inner continental shelf of the southern BCT (Figure 7). Its border fault dips to the east and has a maximum displacement of ~1.5 s. A series of synthetic faults are located east of the border fault. East of the Norfolk Basin, two structural ridges plunge eastward under the outer shelf. It is not clear from the seismic data whether these structures are bounded by faults. About 70 km to the south of the Norfolk Basin lies an ~20 km wide basement depression. Its imaging does not reveal clear faults that might bound it. South of that depression, the top basement is shallower (<3 s), dipping moderately eastward toward the shelf edge. Three elongated rift basins along the northern BCT hinge line that were previously described by Klitgord et al. (1988) and Benson and Doyle (1988) based on seismic reflection data were not identified using the denser data set presented here.

4.2. Base Post-Rift

The general structure of the BPR surface is that of a smooth surface along the top basement, along the top of the rift basins, and along the top of the SDR where these overlay the top basement (Figures 4 and 9). In the GBB area, the BPR descends toward the southeast from less than 0.5 s at the eastern Long Island Platform. Further east, seaward of the Gulf of Maine, the BPR first descends above syn-rift strata of the Inner Yarmouth Basin, forming a trough that plunges to the southwest. East of the Inner Yarmouth Basin, the BPR rises along the top basement of Yarmouth Arch, forming a 170 km long by 70 km wide elongated ridge that also plunges to the southwest (Figures 5 and 7). The BPR then descends to the southeast above the syn-rift strata within the Outer Yarmouth Basin (Figures 5 and 9). The trough above Inner Yarmouth Basin connects to a deeper and wider south trending trough coincident with the Georges Bank Trough (as seen in the top basement map, Figure 7). With travel times of 4.5 s, this is also the deepest part of the BPR under the GBB shelf. The descent from the ~0.5 s deep Gulf of Maine to the deepest trough occurs gradually over ~150 km.

The BPR surface at the Long Island Platform coincides with the top basement where rift basins are absent (Figures 4 and 10). The BPR has a southward plunging convex structure along most of the Long Island Platform (Figures 9 and 10). A steep E-W slope separates the Long Island Platform from the northern BCT.

The asymmetry of the BCT, as observed in the top basement surface, also characterizes the BPR. Similar to the top basement, the BPR morphology shifts from convex (shallower parts) to concave in the deeper areas (Figure 9). The dip in the deepest part of the BPR (> ~ 5 s) is gentler than the dip of top basement in the same locality. The gentler BPR dip is attributed to the filling of the space trapped between the top basement and BPR by SDR and possibly syn-rift strata. (Figures 4, 6, and 8). The BPR at the outer northern BCT reaches more than 6.5 s (Figures 6 and 9). To the south, the BPR dips mostly eastward. The faults, troughs, and highs apparent in the southern BCT top basement have no expression on the BPR.

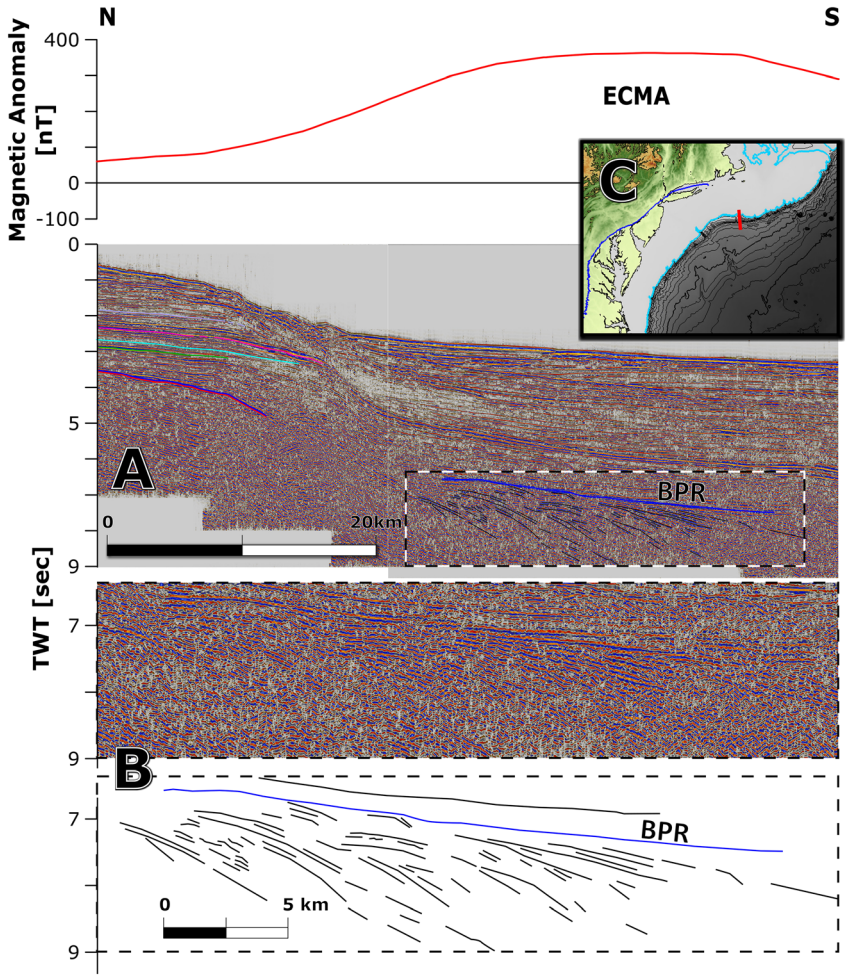

Figure 10. (a) Interpreted dip-oriented time-migrated multichannel seismic profile 288-AN-16744 across the Long Island platform outer continental shelf, slope, and rise. Magnetic anomaly profile is shown across the top of the section. See Figure 3 for description of the stratigraphy. The East Coast magnetic anomaly and the seaward dipping reflectors spatially overlap. Dashed rectangle marks location of B. (b) Magnifications of uninterpreted and interpretation of the part in (a) that show diverging seaward dipping reflectors. (c) Map showing the profile location.

At the onshore Salisbury Embayment, the BPR is concave, deepening toward the BCT (Figure 9). It outcrops at the landward edge of the coastal plain from New York City to the southern extent of the study area and reaches a maximum depth of ~2 s TWT beneath the coastline. In the northern part of the embayment, the BPR forms a concentric structure, plunging toward the central BCT.

4.3. Seaward Dipping Reflectors

SDR appear on seismic data along the entire studied margin. Although their spatial extent and downdip position change along the margin strike, several geomorphic characteristics remain similar. In all the sections that show both SDR and their underlying top basement surface, the SDR packages have a wedge-shaped geometry that thickens seaward and pinches out landward (Figures 6 and 8). The SDR themselves toplap with respect to the BPR. At the GBB and Long Island Platform, the SDR landward termination is 10–30 km seaward of the present-day shelf edge, taken here as the 200 m isobath (Figures 5, 10, 11, and 12). At the BCT, however, the SDR pinch-outs are located more landward, underneath the continental shelf. The landward distance between the pinch-out and the 200 m isobath decreases gradually from ~100 km at the northernmost BCT to ~30 km at the southern BCT. The seaward termination of the packages is less distinctive than their landward termination.

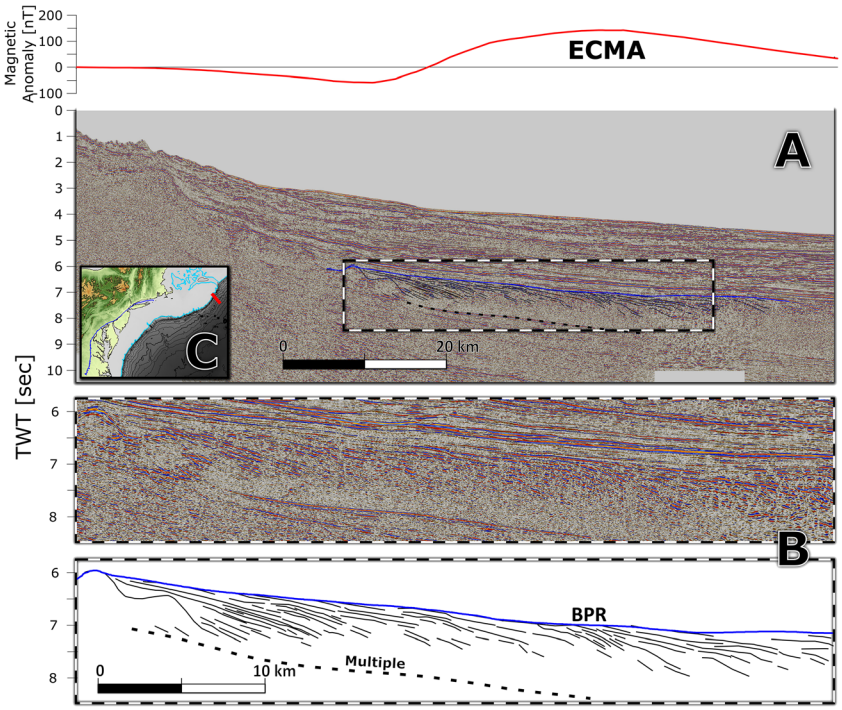

Figure 11. (a) Interpreted dip-oriented seismic reflection section (part of USGS profile 4) across the northern Georges Bank basin continental slope and rise. Magnetic anomaly profile is shown across the top of the section. Dashed rectangle marks location of B. Note the overlap between the East Coast magnetic anomaly and the distribution of seaward dipping reflectors. (b) Magnified seismic expression of the seaward dipping reflectors and its interpretation. (c) Map showing the profile location.

4.4. Moho Depth

Moho reflectors in the USGS seismic lines were identified on dip profiles at the GBB, Long Island Platform, and the southern BCT (Figure 13a). At the GBB, four profiles revealed Moho reflectors at 8–10.5 s (Figures 5 and 13a). Four dip profiles and one strike profile show a relatively continuous series of reflectors at depths of 9–11 s under the Long Island Platform. Moho reflectors are sparsely imaged on the USGS lines covering the BCT. They appear over short distances (tens of kilometers) as discontinuous reflectors on one strike profile and six dip profiles, mostly at the southern BCT.

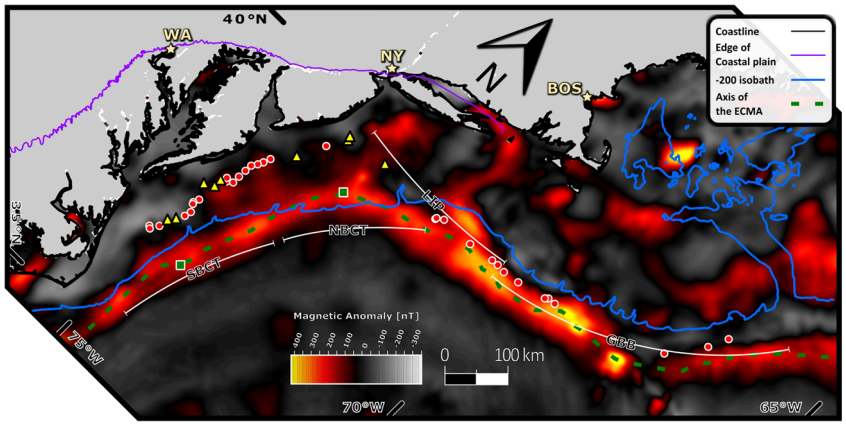

Figure 12. Magnetic anomaly map (adopted from Meyer et al., 2017). Locations of the landward pinch-outs of SDR identified on seismic reflection sections are shown as red circles. Yellow triangles mark the pinch-out location of the base post-rift horizon on seismic sections that do not clearly show an SDR geometry (strike profiles or profiles of insufficient imaging quality). Outlined green squares indicate locations of the seaward limit of the continental crust as observed on seismic refraction data (after Talwani et al., 1995). BOS = Boston; NY = New York; WA = Washington.

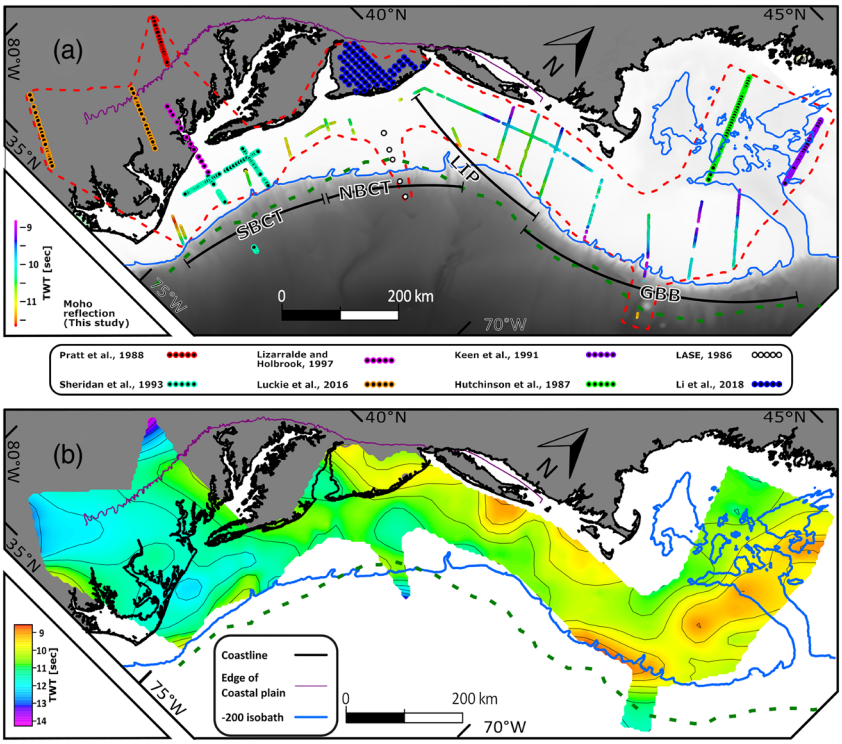

Figure 13. (a) Distribution of data and published results used for constraining base of the crust (the Moho) depths (in two-way travel time). Moho picks (this study) are marked in red-yellow-green-blue-purple spectra. Dashed red polygon marks the area used for interpolation of the Moho depths. Legend shows data sources. (b) Time domain structural map of the Moho interpolated from (a). GBB = Georges Bank basin; LIP = Long Island platform; NBCT = northern Baltimore canyon trough; SBCT = southern Baltimore canyon trough.

Interpolation of interpreted Moho reflectors combined with published Moho picks yielded a regional structural map (Figure 13b). Travel times to the Moho mostly range between 9 to 12 s. At the GBB the interpolated map shows an ~100 km wide by 400 km long ridge in the Moho surface. This elevated Moho extends in a southerly direction from the inner Gulf of Maine to outer GBB and is located mostly in the region between the Franklin Basin and the Inner Yarmouth Basin (Figure 7). The ridge is higher than its surroundings by 1–1.5 s. Under the Long Island Platform, the Moho exhibits general southward dips. Under the offshore portion of the northern BCT the Moho is deeper (~11 s) than under New Jersey coastal plain (~10 s). At the southern BCT, however, there is no clear distinction between the depth to the Moho offshore and onshore.

The heterogeneous distribution of seismic velocities above the Moho may cause the appearance of artificial structures on the TWT structural map. In that sense, the presence of thick, low-velocity sedimentary basins will increase the underlying Moho travel times. Some of the bias is resolved by looking at the crustal thickness map (See description of the BPR to Moho interval and supporting information).

4.5. Isochron Maps

4.5.1. BPR to Moho Interval

The isochron between the BPR surface and the Moho was calculated regionally (Figure 14a). We chose this interval and not the more orthodox top basement to Moho interval for two main reasons. First, the interpretation of the BPR surface is more straightforward than that of the top basement. Therefore, its spatial extent and degree of accuracy are higher, especially where thick syn-rift or SDR successions occur. Second, the use of the BPR as an upper datum for the calculation filters out short-wavelength (<50 km) thickness variations associated with rift basins. These basins manifest crustal deformation restricted to the upper crust that does not necessarily have mantle compensation. The BPR surface smooths these basin structures, thus emphasizing regional crustal thickness variations. The presented thickness could be treated as an upper limit for crustal thickness as the thickness trapped between the BPR and top basement is added to its calculation. On the

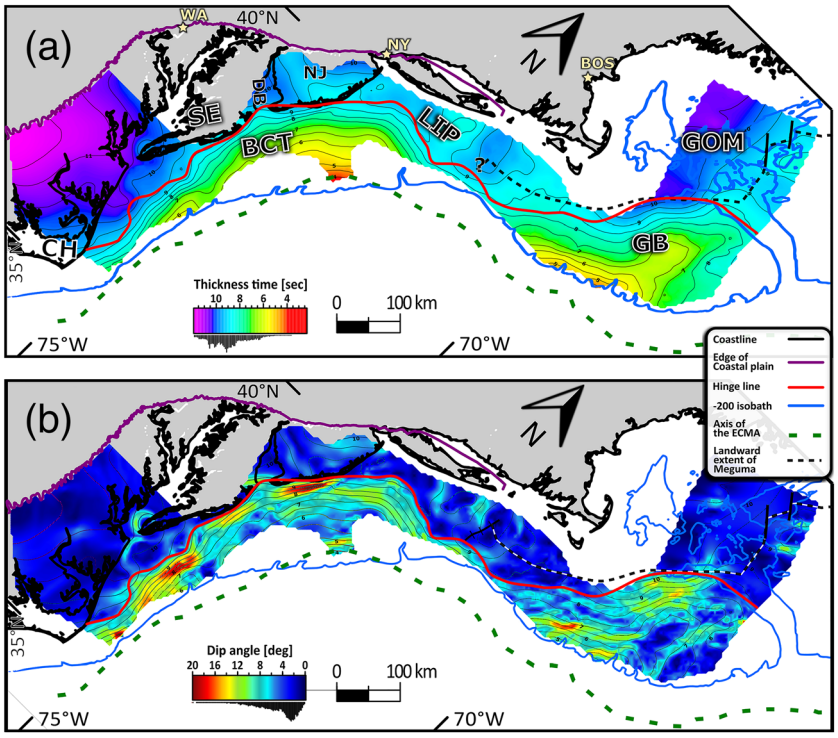

Figure 14. (a) Thickness (in two-way travel time) of the interval between base post-rift and the Moho and (b) gradient of base post-rift-to-Moho thickness expressed as dip angle in degrees, assuming that the Vp of the interval is 6.3 km/s. Contours on both maps represent base post-rift-to-Moho thickness. Red line is the hinge line as defined by the location of increasing base post-rift-to-Moho thickness. Histogram below color scales represents the relative abundance of values. BOS = Boston; BCT = Baltimore canyon trough; CH = Cape Hatteras; DB = Delaware Bay; GB = Georges Bank; GOM = gulf of Maine; NJ = New Jersey; NY = New York, WA = Washington.

deeper troughs (outermost BCT and the GBB trough), the difference between the crustal thickness and BPR to Moho thickness may reach >2 s. This difference nulls where rift basins are absent.

The travel time interval of the BPR to Moho varies along and across the margin. It ranges between extreme values of <4 s at the outer northern BCT to ~12 s landward of southern BCT (Figure 14a). The thickness in ~70% of the region is between 8 and 11 s. GBB is bisected by an NNE-SSW oriented travel time minimum which coincides with Inner Yarmouth Basin and Georges Bank Trough. There, thick syn-rift infill (up to 3 s) with velocities slower than the surrounding basement rocks (<5 km/s for the syn-rift vs. ~6.3 km/s for the continental crust) is expected to increase the travel time interval. This, in turn, causes artificial inflation of the BPR-to-Moho interval. Thus, the thickness minimum under the Georges Bank Trough and Inner Yarmouth Basin is probably even more dramatic than is observed in the time domain. Farther south, toward the GBB shelf edge, the thickness of the interval decreases to less than 5 s.

Unlike the GBB, the Long Island Platform is almost devoid of syn-rift basins with velocities slower than crustal velocities (Figure 7). Travel time crustal thickness at the Long Island Platform, is relatively constant, between 8.5 and 9.5 s (Figure 14a). Similar values extend southwest under the New Jersey coastal plain. At the BCT, the BPR to Moho interval has an asymmetric thickness minimum close to the shelf edge offshore New Jersey. The transition from >9 s thickness at the Long Island Platform and New Jersey coastal plain to the thinnest part at the BCT (<4 s) occurs over less than 110 km. Under the outer southern BCT shelf the interval thickness is 6–7 s; 2–3 s thicker than under the LASE profile ~250 km to the north. The thickness gradient is steepest under the western flank of the southern BCT, where the interval thins by 4 s over ~50 km.

The gradient map of the BPR to Moho travel time thickness shows a "hinge line" where rapid seaward thinning of the crust (in TWT) begins (red line in Figure 14b). The hinge line roughly bounds the BCT and GBB on the west and the Long Island Platform on the east and south. At the BCT, the steepest local gradient is found immediately east of the hinge line.

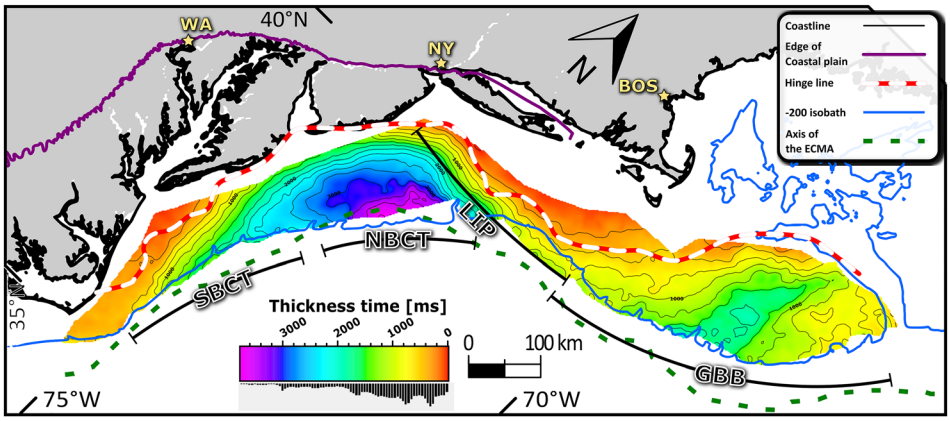

Figure 15. Two-way travel time thickness of the post-rift Jurassic sequence. Histogram below color scales represents the relative abundance of a specific values. BOS = Boston; GBB = Georges Bank basin; NBCT = northern Baltimore canyon trough; NY = New York, WA-Washington.

4.5.2. Early Post-rift

The thickness of post-rift Jurassic sediments, described below, indicates the distribution of the depocenters that developed in the early stages of the drift phase, 30–45 Myr after the continental breakup. Post-rift Jurassic sediments are concentrated in two depocenters under the continental shelf, filling the GBB and the BCT (Figure 15). The GBB depocenter is an NNE-SSW trough with a maximum travel time thickness of ~1.8 s at its southern half. It decreases gradually northward to ~ 1 s at the northern edge of the map. Sediment thickness is much thinner (<800 ms) east of the GBB depocenter. At the Long Island Platform post-rift Jurassic sediments are found only at the outer shelf (Figures 4 and 15). The BCT Jurassic depocenter is asymmetric, thicker in the north (>3.5 s) than in the south. North of there, the Jurassic thins rapidly toward the Long Island Platform (Figures 4 and 15) and pinches out after ~100 km. The western edge of the BCT depocenter is not constrained by the offshore seismic data at the northern BCT.

4.6. Thermal Subsidence and Lithospheric Structure of the GBB

Since the formation of a volcanic margin is to a large extent a thermal process, the rift stage structure of the thermal lithosphere should be examined. To estimate the lithospheric thinning patterns at the time of rifting, we evaluate the thermal relaxation of GBB as expressed by the thickness of the early post-rift sequence. The connection between early post-rift thicknesses and lithospheric thinning is valid assuming that the thinning occurred shortly before breakup and ended with the onset of seafloor spreading (McKenzie, 1978). This assumption is supported by direct age dating of the syn-rift sequence in drill holes at the GBB (e.g., Poag, 1991) and by seismic stratigraphic analysis that shows the rift basins and basement rocks all being truncated by the post-rift unconformity (i.e., BPR in Figures 4 and 5; Klitgord et al., 1988). The inference of a spatial connection between lithospheric thinning and early post-rift depocenter also assumes very low flexural rigidity of the lithosphere. Such low rigidities characterize regions of upwelled asthenosphere (Watts, 1982) and young volcanic margins specifically (Tian & Buck, 2019).

The post-rift Jurassic deposits represent the first 30–45 Myr of deposition on the ENAM after breakup. During this initial post-rift phase where the lithosphere had been thinned, thermal gradients are expected to be steep and thermal subsidence high (McKenzie, 1978). Thermal subsidence indeed peaked during the early post-rift of ENAM, forming most of the Jurassic accommodation space (Poag & Sevon, 1989; Steckler & Watts, 1978). Hence, the post-rift Jurassic thickness (Figure 15) can be treated as a proxy for identifying thermal subsidence patterns and thus areas of lithospheric thinning. Figure 16 shows that the thickness of the BPR to Moho across the GBB is inversely proportional to the thickness distribution of the early post-rift Jurassic unit. For example, areas where the BPR to Moho interval is thinnest (5.8 s, 17.4 km, assuming an average velocity of 6 km/s) are overlain by the greatest thickness of post-rift Jurassic sediments (1.85 s, 4.1 km, assuming an average velocity of 4.5 km/s based on well data [Taylor & Anderson, 1982]). Areas with thicker BPR to Moho (8 s, ~24 km) are overlain by thinner Jurassic strata (0.8 s, ~1.8 km). The spatial relations between crustal thinning and early post-rift thermal relaxation are evident on a map view (Figure 17).

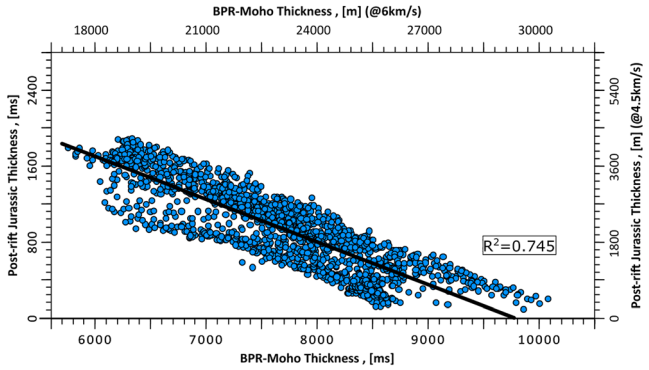

Figure 16. Post-rift Jurassic thickness (in two-way travel time) against the thickness of the base post-rift to Moho interval at Georges Bank basin.

The crustal hinge line outlines the western and northern bounds of the GBB Jurassic depocenter and seemingly the zone of lithospheric necking. This suggested that spatial coincidence of crustal and lithospheric boundaries, together with the thickness relations shown in Figure 16, alludes that thinning of the crust and mantle lithosphere under GBB spatially overlapped. It is possible that not only the crust deformed and thinned over an ~200 km wide zone but so did the lithosphere.

5. Discussion

5.1. Breakup Volcanism, the East Coast Magnetic Anomaly, and the Width of the Extended Continental Crust

The final stages of the formation of the ENAM were accompanied by voluminous magmatic eruptions and the emplacement of the ECMIP. The results presented here show that the landward extent of the volcanism, as marked by the pinch-out location of the SDR wedge, spatially correlates with the western limit of the ECMA (Figures 5, 6, 8, 10, 11, and 12). This observation supports previous correlations that were based on a few isolated 2-D seismic lines (e.g., Austin et al., 1990; Holbrook & Kelemen, 1993). However, the relationship between the landward extent of the SDR wedge and the corresponding magnetic anomaly varies along the margin. Whereas at the GBB and the Long Island Platform the SDR pinch-out correlates with the landward edge of a narrow (~80 km) high-amplitude anomaly that is regarded as the axis of the ECMA (Behn & Lin, 2000; Benson & Doyle, 1988; Klitgord et al., 1988), at the BCT, and in particular at its northern part, the SDR terminate where a low-amplitude extension of the anomaly feathers out (Figures 6 and 12). It is noteworthy that this extension also appears in a reduced to pole version of the magnetic anomaly map, as presented by Behn and Lin (2000).

To evaluate the extent of crustal thinning west of the breakup line, it is crucial to define both the landward and seaward bounds of the area of thinned continental crust. Rift structures are widely spread (up to 400 km) between the eastern Appalachians and the continental slope (Figure 2; Withjack et al., 2012). Yet onshore rift basins usually overlay continental crust of normal or thicker-than-normal thickness (>35 km, Li et al., 2018). Stretching in these areas appears to be restricted to the upper crust and does not involve local mantle compensation (Harry & Sawyer, 1992; Li et al., 2018; Sawyer & Harry, 1991). Most of the thinning occurs farther seaward, along a margin-parallel belt (Figure 14). While the data presented here provide a good estimate of the landward boundary of this thinning belt (i.e., the hinge line, Figure 14), its seaward

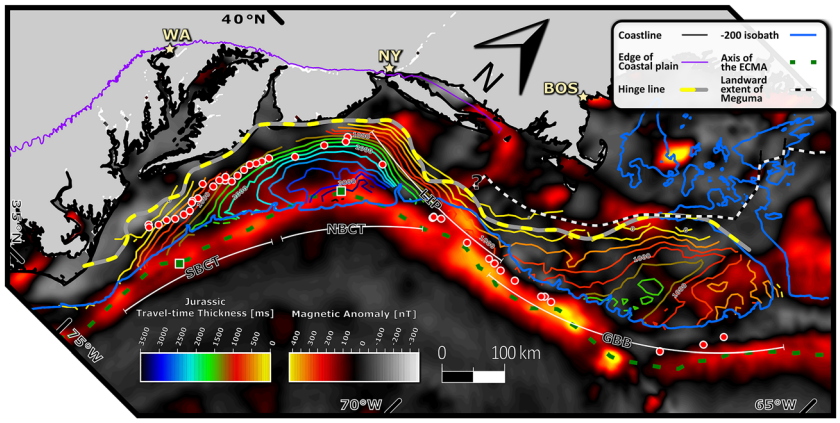

Figure 17. Magnetic anomaly map (Meyer et al., 2017) overlaid by key results, including location of the hinge line, locations of the SDR landward pinch-out (red circles), and Jurassic thickness contours (colored according to a thickness spectrum). Green squares mark locations of the seaward limit of the continental crust as observed on seismic refraction data (after Talwani et al., 1995). BOS = Boston, GBB = Georges Bank basin; LIP = Long Island platform; NBCT = northern Baltimore canyon trough; NY = New York; SBCT = southern Baltimore canyon trough; WA = Washington.

edge, where the crust turns entirely igneous, is more elusive (for further discussion regarding the challenges in determining the edge of the continental crust see Eagles et al., 2015). The high-amplitude pick of the ECMA was previously regarded as the approximate position of the seaward edge of the continental crust (i.e., ocean-continent transition; e.g., Austin et al., 1990; Greene et al., 2017; Klitgord et al., 1988; Withjack et al., 2012). In addition, interpretations of refraction profiles along the ENAM suggest that the crust located seaward of the ECMA axis is entirely igneous or oceanic (Figures 6, 8, and 12; Austin et al., 1990; Holbrook et al., 1994; Shuck et al., 2019; Talwani et al., 1995; Talwani & Abreu, 2000). Considering the paucity of available refraction data, the ECMA is assumed here to mark the seaward edge of the continental crust. Therefore, the crust in the area bounded by the hinge line and the axis of the ECMA is considered thinned continental crust, probably intruded, and partially overlaid by breakup volcanism. The width of this area, when measured perpendicular to the ECMA, reaches ~220 km at the GBB and ~110 km at the northern BCT (Figure 12). It is narrowest at the Long Island Platform and southernmost BCT where it extends for ~60 km.

5.2. Along Margin Variability: Key Differences Between the Segments

Our data reveal an along-margin variability in crustal structure, deformation style, volcanic addition and post-rift sedimentation of the ENAM. The variability is especially noteworthy between the GBB and the BCT, two parallel segments, oriented perpendicular to the rifting-related extensional regime (Withjack et al., 2012). Variations are manifested in several ways: (a) whereas a narrow band of thinned continental crust lies seaward of a steep hinge zone at the BCT (<110 km), a gentle hinge zone borders a wide (up to 220 km) thinned zone at GBB; (b) few rift basins are observed at the BCT, whereas a complex system of well-developed rift basins and detachment faulting constitutes the base of GBB; (c) volcanism in the form of SDR at the BCT reaches landward <50 km east of the hinge line, whereas the landward boundary of the SDR at GBB is located much farther seaward under the continental rise, separated from the hinge line by up to 200 km; (d) the early post-rift sediment fill of the BCT consistently thickens seaward, whereas at the GBB the thickness increases toward the middle shelf and decreases again toward the Yarmouth Arch (basement high) under the outer shelf.

A broad zone of thinned crust landward of the ECMA is also observed in the volcanic Scotian margin of Canada, immediately north of the GBB (Figure 2; Deptuck & Kendell, 2017; Savva et al., 2016). Water depth at the Scotian margin reaches ~2.5 km (Savva et al., 2016), Jurassic sediment thickness is ~3 km (Deptuck & Kendell, 2017), and crustal thickness is 20 km (Dehler, 2012). It, therefore, appears that a broad zone of crustal and likely lithospheric thinning landward of the magmatic outpouring extends along a substantial (650 km) portion of the Atlantic margin, which includes both the GBB and the volcanic SW most Scotian margin.

The Long Island Platform, located between the GBB and BCT, has a relatively thick crust (8–10 s or ~31–25 km), few extensional structures, and minor early post-rift subsidence (0–3 s or 0–5 km top basement depth; Figures 4 and 7). Its hinge line, top basement dip, and ECMA trend are oblique to those found at BCT and the GBB. At the eastern Long Island Platform, the BPR-to-Moho interval maintains its thickness from the inner shelf to the shelf edge (Figure 14a) and forms a steep BPR-to-Moho hinge, about 50 km away from the ECMA and the SDR. The obliquity of the Long Island Platform, relative to its neighboring segments and the minor thinning of its crust, was previously interpreted as the result of transform or wrench motion during rifting (Hutchinson & Klitgord, 1988; Klitgord & Behrendt, 1979; Klitgord et al., 1988; Thomas, 2006). Some have linked the obliquity of the Long Island Platform and its suggested transform motion to the intersection of the margin at this segment by oceanic fracture zones (Klitgord et al., 1988; Le Pichon & Fox, 1971). Yet recent studies have rejected the genetic connection between oceanic fracture zones and syn-rift strike-slip faults (e.g., Taylor et al., 2009). While tensile strain in an oceanic lithosphere tends to localize in an orthogonal or parallel direction (Dauteuil & Brun, 1996), strain in a continental lithosphere may be accommodated by oblique rifting (e.g., Gulf of California (Bennett & Oskin, 2014) and Gulf of Aden (Autin et al., 2013)). Thus, inference regarding the transform nature of the Long Island Platform cannot be based solely on its spatial relation to oceanic fracture zones. The intrinsic characteristics of the Long Island Platform do not match these expected from a transform margin. It lacks fundamental structures of transform margins such as a marginal ridge, continentward tilted horizons, and a marginal plateau (Mercier de Lépinay et al., 2016). On the other hand, the presence of a sharp hinge, minor crustal thinning, and

post-rift subsidence fits an obliquely rifted margin (Davison, 1997). From a kinematic perspective, the Long Island Platform might have served as an accommodation/transfer zone (e.g., Morley et al., 1990; Schlische & Withjack, 2009) between two orthogonal rift segments.

5.3. Examination of Models for the Creation of Volcanic Margins

Models of magmatic rifting and volcanic margin formation predict a narrow zone (<100 km) of crustal and lithospheric thinning and steep relief at the base of the lithosphere. The narrow geometry is considered to be either the result of weakening and localizing processes that stem from the steep geothermal gradient at volcanic rifts (Buck, 2004, 2006; Geoffroy, 2005; Geoffroy et al., 2015; White & McKenzie, 1989) or the initial conditions required for melt generation (Mutter et al., 1988; Simon et al., 2009; Van Wijk et al., 2001). The proposed models are supported by globally distributed observations of narrow volcanic margins (e.g., Franke, 2013; Franke et al., 2007; Hopper et al., 1992; Hopper et al., 2003; Paton et al., 2017; Schnabel et al., 2008; Tréhu et al., 1989) including the crustal structure of the BCT (Figures 6, 8, and 14; Holbrook et al., 1994; LASE, 1986; Lizarralde & Holbrook, 1997).

Although the GBB is volcanic, it does not fit the observations and models of a narrow thinning zone that is usually ascribed to volcanic margins. The observations presented here indicate an ~220 km wide zone of crustal thinning at the GBB (Figures 5, 7, and 14). The thinning is manifested by well-developed brittle extensional structures possibly coupled with ductile deformation of the middle crust (or below). The crust is considerably thinner than typical continental crust (35–40 km; Christensen & Mooney, 1995) and reaches a minimum thickness of 4–6 s or 12–19 km, assuming an average crustal Vp of 6.3 km/s (Figures 5 and S1 in the supporting information). The wide extent of thinned crust, together with the presence of middle crust detachment faulting and developed surface extensional structures, is usually ascribed to magma-poor margins. At such margins, the zone in which such features occur is referred to as the "necking domain" (Peron-Pinvidic et al., 2013; Reston, 2009; Sutra et al., 2013). The necking domain represents a thinning phase during which strain localization and deformation of the middle and possibly lower crust occurs, promoting drastic crustal thinning. In the sequence of events that leads to the formation of magma-poor margins, thinning follows a phase of tectonic stretching that is locally uncompensated by mantle uplift (i.e., "stretching phase") and predates hyperextension of the crust and exhumation of mantle rocks (i.e., "hyperextension/exhumation phase"; Peron-Pinvidic et al., 2013). The juxtaposition of a wide necking domain and SDR makes the structure of the GBB (and likely also the southwest Scotian margin) a hybrid between an underdeveloped magma-poor margin and a volcanic margin.

The broad (>200 km) syn-rift thinning under the GBB challenges the understanding of the thermomechanical conditions suggested for the formation of volcanic margins. The initial conditions required for a volcanic breakup, as proposed by Mutter et al. (1988), include a sharp near-vertical asthenosphere-lithosphere boundary that would induce convective partial melting. This condition was most probably not met at the GBB where the relief of the base of the thermal lithosphere was moderate and thinning of the lithosphere probably took place over 200 km across the margin. Buck (2004, 2006) proposed that a considerable amount of lithosphere extension over a hotter-than-normal asthenosphere would be accommodated by dike intrusions. Moreover, high heat flux around the intrusions would weaken the lithosphere and promote strain localization toward the rift axis. This mechanism would result in a minor and localized thinning. Although this model might successfully explain the narrow structure of the BCT, it fails to explain the broad necking zone under GBB. Kelemen and Holbrook (1995) also proposed that lithospheric necking was minor prior to the formation of the volcanic BCT and originated in melts formed under high pressure (up to 4 GPa) and temperatures, which they attributed to the presence of a thick lithospheric lid above the melt. At the GBB, however, premagmatic necking reduced the thickness of such a lid. Geoffroy et al. (2015) emphasized the role of continentward dipping detachment faults play during crustal necking at volcanic margins. The abundance of oceanward dipping faults at the GBB (Figure 7), the ~200 km offset between the crustal necking and the ECMIP (Figure 17), and the lack of evidence supporting continentward dipping faults associated with the SDR along the entire ENAM (Figures 8, 10, and 11; Lizarralde & Holbrook, 1997) do not support the model proposed by Geoffroy et al. (2015).

A possible reconciliation between lithospheric thinning and the melting under high pressure might include a time-varying geotherm. In this scenario, initial rifting would take place over a "cold" mantle (potential temperature is <1300°C, Reston, 2009) forming a wide, magma-poor structure. If mantle temperature

were to rise later, this magma-poor structure would be superimposed by a narrower volcanic structure. If this is the case for the rifting of the GBB, then the increase in mantle temperature is not expected to result from the geometry of the rift as in the edge-driven convection models (King & Anderson, 1998; Mutter et al., 1988). Similarly, elevated mantle temperature could not be related to a heated pre-rift mantle such as in the continental insulation models (e.g., Anderson, 1982; Brandl et al., 2013; Hole, 2015) since the initial rifting took place over a cold mantle. Rather, it should stem from processes not related to the rift itself, such as a mantle plume (White & McKenzie, 1989). If, as some suggested, the plume was situated at the southern part of the rift (Ruiz-Martínez et al., 2012; Wilson, 1997), the amount of magmatic additions to the margin should decrease northward. Yet the intensity of the ECMA does not decay northward (Figure 2). Since the amplitude of the ECMA correlates with the added magmatic volume (Holbrook & Kelemen, 1993; Talwani et al., 1995), there is also no sign of northward decrease in the volume of the breakup magmatism. The independence of the reduced-to-pole ECMA and the SDR burial depth supports the connection between the intensity of the ECMA and the volume of the volcanic rocks (Figures 7b and 7c in Behn & Lin, 2000). Moreover, some geochemical (Whalen et al., 2015; Shellnutt et al., 2018; Elkins et al., 2020) and geophysical (Shuck et al., 2019) evidence cast doubt on a mantle plume origin of CAMP and ECMIP melts. Other mechanisms such as volatile enrichment of the mantle (Elkins-Tanton, 2007) and slab breakoff (Elkins et al., 2020; Whalen et al., 2015) may also explain the sudden initiation of magmatism. Unfortunately, these cannot be confirmed or disproved using the data presented here.

The eastern North Atlantic volcanic margin in northern Europe was formed by successive rifting events dating from the Late Devonian to the early Cenozoic volcanic breakup (Doré et al., 1999; Roberts et al., 1999). This led some authors to suggest that wide rifting, like rifting that predates to the formation of magma-poor margins, also predates the formation of volcanic margins (Eldholm et al., 1995, 2000). However, the protracted nature of rifting of the eastern north Atlantic implies that although the crust under that margin was thin, the lithosphere was not necessarily thin at the onset of rift magmatism. Cooling of upwelled mantle between rifting phases should have resulted in the rethickening of the lithosphere. Unlike the European North Atlantic, the Central Atlantic, and the ENAM in particular, had experienced a relatively short and continuous rifting that was immediately followed by seafloor spreading (Withjack et al., 2012). Recently, Guan et al. (2019) proposed that volcanic margins that experienced nonmagmatic rifting shortly before their volcanic breakup exhibit narrow necking zones, whereas longer time spans between failed rifting and volcanic breakup result with wide volcanic margins. This is in contradiction with the observed variations between the GBB and BCT, which experienced similar rifting histories before their volcanic breakup.

The African side of the Atlantic South Austral margin is a possible example of a volcanic margin that was tectonically thinned soon before its magmatic phase. Like the GBB, the southernmost part of the margin exhibits a wide area of thinned continental crust, high-strain extensional structures, and detachment faulting along with SDR that correlate with a prominent magnetic anomaly (Blaich et al., 2011). The geometry of the adjacent segment to the north exhibits the typical narrow and steep margin. Examining the Brazilian margin, Stica et al. (2014) interpreted a 280 km wide zone of necked and intruded crust between the hinge line and the first oceanic crust of the Pelotas Basin. Yet unlike the GBB, most of this zone underlies a thick SDR wedge, which the authors interpret as "continental igneous crust". A modern analog for the rifting of the GBB may be found at the Manda Hararo active rift in central Afar. There, Stab et al. (2016) observed a wide zone (~200 km) of crustal necking, midcrustal detachment faulting along with abundant volcanism.

Although it is clear from our results that the style of thinning varied along the ENAM, the causes for these variations remain unsettled. Trying to explain the difference in crustal structure and post-rift subsidence, Klitgord et al. (1988) and Wernicke and Tilke (1989) proposed a simple shear model (Lister et al., 1991; Wernicke, 1985) with alternating polarities between the segments. Modeling efforts have shown, however, that simple-shear rifting does not allow enough melt production for the formation of volcanic margins (Buck et al., 1988; Latin & White, 1990; Simon et al., 2009). More recent numerical modeling addressed the width of the lithosphere necking zone at rifts and passive margins (e.g., Svartman Dias et al., 2015; Tetreault & Buiter, 2018). According to these models, two main factors appear to determine the architecture of a rift system: the extensional strain rate and the rheology of the lithosphere. Estimates of syn-rift divergence rates at ENAM range between 2 and 6 mm/year for the Carolina Trough (Kneller et al., 2012; Ruiz-Martínez et al., 2012, respectively) to 8 mm/year for the BCT (Schettino & Turco, 2009).

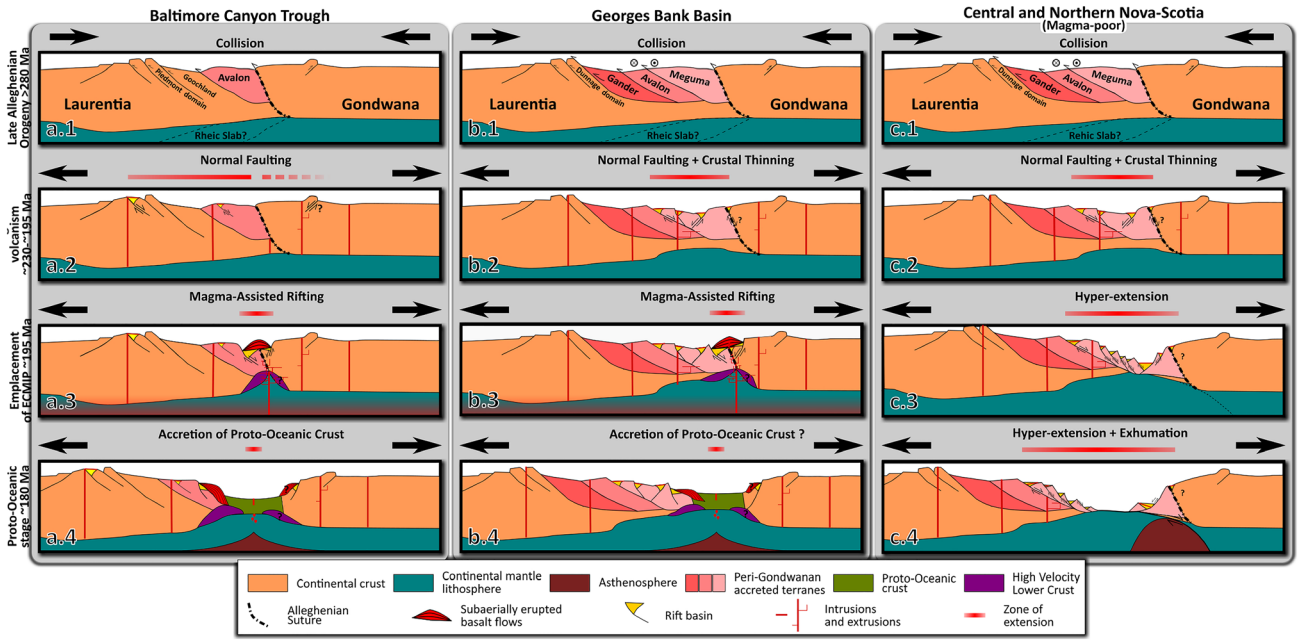

Figure 18. Schematic model for the formation of ENAM along the BCT (a), GBB (b), and central and northern Nova Scotia (c) segments (not to scale). Where Meguma terrane is present, it focused the premagmatic extensional strain. Strain had localized oceanward when rifting at the BCT, and the GBB turned magmatic. General pre-rift crustal configuration of ENAM follows Hatcher et al. (2010) and Hibbard et al. (2006). Specific additions include the BCT crustal composition (Sheridan et al., 1993), the extension of Laurentia under the peri-Gondwanan terranes (Cook & Vasudevan, 2006; Marzen et al., 2019; Pratt et al., 1988), the nature of the Gondwanan crust (Le Roy & Piqué, 2001; Villeneuve, 2005), the structural relations between Avalon and Meguma terranes (Hutchinson et al., 1988; Keen et al., 1991; Pe Piper & Jansa, 1999), the protooceanic stage structure of the BCT (Biari et al., 2017; Labails et al., 2009; LASE, 1986; Lizarralde & Holbrook, 1997; Shuck et al., 2019), GBB (Dehler, 2012) and central and northern Nova Scotia (Klingelhoefer et al., 2016; Maillard et al., 2006; Wu et al., 2006) segments, the role of the Alleghenian suture as a magma conduit during the emplacement of ECMIP (McBride & Nelson, 1988), and the possible existence of a Rheic slab under Laurentia (van Staal et al., 2009; Whalen et al., 2015).

The margin-wide distribution of slow to ultraslow divergence of similar orientation cannot account for the lateral variation in margin architecture. Thus, we suggest that rheological rather than kinematic contrasts were dominant in shaping the margin's width.

5.4. The Origin of Along-Margin Variability at the ENAM

Previous interpretations and numerical modeling of the rifting and breakup of the Central Atlantic margin mostly assumed initial conditions of homogenous rheology of the continental lithosphere subjected to tensile stresses and perhaps underlying heat and melt source (Dunbar & Sawyer, 1989; Klitgord et al., 1988; Wernicke & Tilke, 1989). Furthermore, most margin-scale rifting models lack the crustal and likely lithospheric lateral heterogeneity as manifested in the crustal fabric of eastern North America and the time-varying geotherm imposed by the emplacement of CAMP and ECMIP. The lithosphere in which rifting and breakup occurred was the outcome of ~160 Myr of west dipping subduction, collision, and right-lateral translation (Hatcher et al., 2010; Hibbard et al., 2007, 2010; van Staal et al., 2009). The convergence phase ended with the collision of Gondwana along the Rheic/Allegahanian suture at ~280 Ma, leaving a heterogenous pre-rift lithosphere (Figures 2b and 18). In addition to the spatial rheology variations, the introduction of heat by the emplacement of CAMP and ECMIP added a time-varying component to the rheological structure of the lithosphere (Kelemen & Holbrook, 1995; Marzoli et al., 1999). To try and address these complexities, we first examine the along-strike variability of ENAM's crustal building blocks and their response to the premagmatic rifting and later examine the effect of magmatism on the rift architecture.

5.4.1. Rheological Controls on the Premagmatic Rifting

Examining the pre-rift crustal fabric reveals major compositional differences along the strike of the ENAM. The outboard portion of the Appalachian crust is composed of peri-Gondwanan Terranes that were accreted to Laurentia before the Alleghenian orogeny. Meguma terrane at the northern part of the margin (Figures 2, 18b, and 18c) is the easternmost and latest accreted terrane to Laurentia (Hatcher et al., 2010; Hibbard

et al., 2007). Exposed in Nova Scotia, the Meguma terrane overthrusts the Avalon terrane to the NW (Figures 18b and 18c). The Avalon terrane overthrusts the Gander terrane from New England to Newfoundland but probably abuts the older Appalachian belts (the Goochland or Piedmont domains) landward of the BCT (Figures 2 and 18a; Hatcher et al., 2010; Hibbard et al., 2006; Sheridan et al., 1993). Basement rocks under the GBB and the Scotian Shelf are interpreted to belong or be closely related to the Meguma terrane (Hutchinson et al., 1988; Kuiper et al., 2017; Pe Piper & Jansa, 1999). To the south, the Avalon Terrane was suggested to underlie the BCT constituting the most outboard Paleozoic terrane of this segment (Hatcher et al., 2010; Sheridan et al., 1993).

The Meguma and Avalon terranes have different compositions. The Meguma terrane is composed of 10–12 km of metasedimentary sequence (White et al., 2010) that overlies crystalline rocks of Gondwanan passive margin affinity. Both metamorphic and crystalline rocks are intruded by mostly felsic plutons of Devonian age (van Staal et al., 2009). The Avalon terrane is composed of several arc-related volcano-sedimentary belts. The oldest exposed Avalonian rocks in Newfoundland represent oceanic crust and are composed of plutonic and volcanic rocks of gabbroic composition (O'Brien et al., 1996). These rocks are overlain and intruded by Neoproterozoic sediments and arc-related magmatic rocks of bimodel composition (O'Brien et al., 1996; van Staal et al., 2009). Although a full lithological description of the two terranes is lacking, the thick metasedimentary sequence and presumably felsic basement of the Meguma terrane should result in a weaker rheology compared to the rheology expected from the intermediate-mafic Avalonian composition.

The compositional differences between the terranes were manifested during the premagmatic Mesozoic extension. In areas where the two terranes juxtapose, extension-related crustal thinning remained confined to the Meguma terrane. Inboard of the Meguma-Avalon suture, the Avalon terrane is observed to be mostly unbroken and unthinned (Figures 18b and 18c). For example, Pe Piper and Jansa (1999) showed that crustal necking offshore Nova Scotia was limited to the Meguma basement. Similar relations exist farther south between the unthinned Avalon crust of the Gulf of Maine and the thinned Meguma crust under the GBB (Hutchinson et al., 1988; Keen et al., 1991). Our suggested hinge line in the GBB coincides with the Hutchinson et al. (1988) and Keen et al. (1991) boundary between the Avalon and Meguma terranes (Figure 14) and implies that the Meguma terrane had a weaker, more easily deformed crust in which extensional strain concentrated. More generally, where the ENAM included the Meguma terrane, the distribution of rift basins is restricted to the Meguma belt (Figures 2, 18b, and 18c). Where the Meguma terrane is absent and the Avalon terrane constitutes the outboard terrane, rift basins developed farther inland on top of older Appalachian domains (Figures 2 and 18a; Hatcher et al., 2010). If our hypothesis is correct, the weaker Meguma terrane accommodated the extensional stresses, whereas the stronger Avalon terrane resisted the extensional deformation and transferred the stress to adjacent areas. Furthermore, post-CAMP intrusions faulting at the rift basins onshore the BCT (Withjack et al., 2012) implies that strain localization and thus necking (Buck et al., 1999) of the crust under the BCT did not occur earlier than 200 Ma. We argue that the necking of the BCT was made possible only when rifting was magma assisted, later than ~195 Ma (see later discussion).

The weaker inherited rheology of the GBB allowed rifting to progress from stretching to necking without the need for magmatic softening. The weak Meguma rheology facilitated deep detachment faulting, shearing, and ductile behavior of the middle to lower crust (Figure 5) along with intense brittle deformation of the upper crust (Figure 7). The fault-bounded rift basins in the GBB are coincident with the zone of crustal thinning. The age of these basins is considered pre-SDR (Carnian-Norian age: 237–208.5 Ma; Poag, 1991). Thus, the 200 km wide crustal and possibly lithospheric necking zone observed at the GBB resulted from premagmatic rifting. The presence of the weak rheology of the Meguma terrane probably enabled wide necking (Svartman Dias et al., 2015). Thus, we propose that a composition-controlled strain distribution determined the along-margin variations in the premagmatic necking stage as observed on our data.

5.4.2. Magma-Assisted Rifting at ENAM

The Eastern North American Rift System entered its magmatic phase with the emplacement of CAMP at ~200 Ma, 40–30 Myr after rifting began. Fault-controlled subsidence onshore the BCT segment mostly ceased a few Myr after the emplacement of CAMP (Withjack et al., 2012). The abandonment of faults landward of the ECMIP in conjunction with the initiation of volcanism is also observed at the GBB. There, the SDR emplacement follows the post-rift unconformity (Klitgord et al., 1988). Le Roy and Piqué (2001) describe oceanward migration of strain simultaneously with volcanism at the African conjugate of

ENAM. Early passive margin models would attribute the cessation of faulting to the onset of seafloor spreading (Falvey, 1974; McKenzie, 1978), suggesting that the emplacement of CAMP and the SDR is related to the initiation of seafloor spreading. However, Shuck et al. (2019) and Kelemen and Holbrook (1995) showed that the generation of the magmas that formed ECMIP and the subsequent proto-oceanic crust took place under a lithospheric lid 15–70 km thick. In other words, the tectonic transition associated with the emplacement of the ECMIP does not signify the breakup of the lithosphere or the rift drift transition but rather a change in nature of strain accommodation that was from this point dominated by the intense magmatism instead of faulting.

Models predict that dike intrusion would reduce the tectonic force required for mechanical stretching and promote strain localization, thus narrowing a rift system (Buck, 2004, 2006; Buck et al., 1999). The reduction in lithospheric strength is attributed to heating caused by the magmatic intrusions. The applicability of the suggested relationship between the magmatism of the rift and strain localization at ENAM could be examined by comparing its volcanic and magma-poor segments. The ENAM volcanic to nonvolcanic transition occurs north of the GBB, offshore southern Nova Scotia (Figure 2; Keen & Potter, 1995; Dehler, 2012; Deptuck, 2020). The rift basins north of the transition and landward of the ECMA (Fundy, Mohican, and Orpheus basins) continued accumulating sediments 5–25 Myr after the emplacement of CAMP (Withjack et al., 2012). That is, strain localized and faulting ceased only in segments where CAMP magmatism was followed by magmatic rifting associated with the emplacement of extrusive basalts (SDR). Similar magmatic localization occurred at the Afar region in east Africa where localized volcanism replaced faulting along widely distributed border faults (Keir et al., 2006; Wolfenden et al., 2005).

The crustal structure of the BCT fits observations at the currently active magma-assisted East African Rift. The necking zone of the BCT is narrow (80–110 km) and is overlaid by SDR. The hinge line roughly parallels the landward edge of the SDR alluding to a genetic relation between volcanism and crustal thinning (Figures 6, 8, and 17). Similarly, at the northern part of the East African Rift, zones of localized crustal thinning overlap areas of voluminous basaltic flows interpreted as early-stage SDR (Bastow & Keir, 2011). To explain the tight connection between volcanism and crustal thinning, Bastow and Keir (2011) proposed that initially, repetitive, localized magmatic intrusions reduced lithospheric strength without reducing crustal thickness. Once sufficiently weakened, the lithosphere thinned mechanically along a narrow band. The narrow thinning resulted in decompression melting and extrusion of voluminous basaltic flows above the area of intruded and thinned continental crust. The BCT crustal structure and its relation to the distribution of SDR lead us to suggest that a similar sequence of events occurred during the ENAM magmatic phase.

With the transition to the magmatic phase later than 200 Ma, the dominant factor in determining the rheology, and thus the locus of straining, was no longer the composition of the crust but the strength reduction by magmatic intrusions. At this stage, the rift basins west of the ECMA were abandoned and strain migrated toward areas weakened by diking and heating (Figures 18a.3 and 18b.3). Therefore, the structures inboard of the ECMA represent the premagmatic deformation, whereas the structures overlapping ECMA resulted from superposition of premagmatic and magmatic rifting. Offshore central and northern Nova Scotia, where the rift never turned magmatic (Keen & Potter, 1995), crustal thinning continued after 200 Ma as indicated by the presence of hyperextended crust offshore (Figure 18c.4; Funck et al., 2004; Wu et al., 2006). An alternative explanation for continued rifting in central and northern Nova Scotia up to ~175 Ma was that the breakup was diachronous being earlier in the south than in the north (Withjack et al., 2012). Recent work by Shuck et al. (2019) suggests, however, that extension without seafloor spreading also persisted until around that time (175 Ma) offshore Cape Hatteras, just south of our study area. Therefore, the breakup does not appear to have been diachronous.

5.4.3. Rheology and Across-Ocean Asymmetry

The previous paragraphs discussed the along-strike heterogeneity of the ENAM. Recent studies of the west African margin show that the structure also varies between the conjugate pairs across the Atlantic Ocean (e.g., Labails et al., 2009; Biari et al., 2017: Klingelhoefer et al., 2016). The African conjugate of the BCT has a narrower necking zone, more moderately thinned crust, and fewer or no SDR compared to the BCT (Biari et al., 2017; Labails et al., 2009). Data regarding the crustal structure of the conjugate of the GBB are lacking. The Moroccan conjugate of northern Nova Scotia is also narrower and thinner than its American pair (Biari et al., 2017). Similar to the ENAM, the African conjugate underwent oceanward strain localization associated with late Triassic-early Jurassic volcanism (Le Roy & Piqué, 2001).

We speculate that, also like the ENAM, the African inherited pre-rift rheology determined the nature of the premagmatic rifting. We propose that the structural asymmetry might reflect the asymmetry in rheological properties between the conjugate pairs. Following a prolonged history of westward subduction and collision, the Permian North American side of the rift was made of a series of peri-Gondwanan accreted terranes overlying a wedge of Laurentian (Grenville) crust that thinned toward Gondwana (Figure 18; Hibbard et al., 2006; Hatcher et al., 2010; Cook & Vasudevan, 2006; Sheridan et al., 1993; Sheridan et al., 1999, Hughes & Luetgert, 1991; Marillier et al., 1989). The Rheic/Alleghenian suture separated the peri-Gondwanan terranes from the overthrusted African Craton (McBride & Nelson, 1988; Villeneuve, 2005). McBride and Nelson (1988) suggested that breakup and the emplacement of the ECMIP followed the Rheic/Alleghenian suture and the suture served as a zone of weakness during the Mesozoic rifting (Figures 18a.3 and 18b.3). The coincidence of the ECMIP with the suture would have left the Appalachians and their accreted terranes on the Laurentian (North American) side of the ocean and the African Craton on the Gondwanan side. If premagmatic extensional deformation concentrated on the peri-Gondwanan terranes (see previous discussion) and other Appalachian weakness zones, then the African side of the rift should have remained mostly unthinned. A full model describing the interaction between the dying convergent Paleozoic boundary and the birth of the Mesozoic ocean is beyond the scope of this paper. However, we note that such model will have to consider the inherited asymmetry and the uneven distribution of the crustal and lithospheric rheology.

6. Conclusions

A full crustal model of the ENAM shelf from Cape Hatteras to the United States-Canada border was constructed and incorporated with seismic interpretation and mapping of upper crustal structures, breakup volcanism, and early post-rift sedimentation patterns to examine the nature of the premagmatic thinning of the crust and mantle lithosphere in a volcanic margin setting. The results are based on seismic interpretation of more than 64,000 km of seismic reflection profiles tied to 40 wells and of published data. Dense data and newer processing and visualization techniques provided significantly more detailed crustal and fault structures of the ENAM shelf than was previously available. We found that the structure of the southern and northern BCT is typical of a volcanic continental margin with a narrow (~50 km) transition zone between a normal thickness continental crust and the breakup volcanism. The crustal structure of the GBB shows a broad zone (≤200 km) of crustal thinning landward of the SDR inferred to be coupled with a broad zone of lithospheric thinning. To explain these differences, we divide the rifting into premagmatic (prior to the emplacement of ECMIP) and magma-assisted rifting. While the GBB underwent intense premagmatic thinning, the BCT experienced no or minor thinning prior to the emplacement of ECMIP. We suggest that the nature and vigor of premagmatic rifting were determined by the spatial distribution of the pre-rift crustal rheology. Weaker rheology of the Meguma terrane underlying the GBB allowed intense faulting and crustal thinning, whereas the stronger rheology of the Avalon terrane underlying the BCT inhibited crustal thinning and transferred the tensile stresses westward to the older Appalachian domains. Magma-assisted rifting started with the emplacement of ECMIP (later than 200 Ma). It included localized magmatic heating and intrusion. Heating overwhelmed the compositional constraints on the rheology and facilitated oceanward strain localization. Localized straining resulted in a narrow necking zone overlaid by SDR. We speculate that the cross-ocean asymmetry in deformation and magmatism between the passive margins of Africa and North America may have also been governed by the heterogeneous distribution of the rheology.

Data Availability Statement

The seismic reflection data included in this study are available online (https://walrus.wr.usgs.gov/namss/search/).

Acknowledgments

Financial support was provided by the U.S. Department of Energy Award DE-FE-0026087 to Battelle Memorial Institute under the "Mid-Atlantic U.S. Offshore Carbon Storage Resource Assessment" Project. We gratefully acknowledge discussions and data exchange with project leaders and participants Ken Miller, Dave Goldberg, Will Fortin, Kim Baldwin, Chris Lombardi, John Schmeltz, Leslie Jordan, Neeraj Gupta, Isis Fukai, Peter McLaughlin, and Mojisola KunleDare. Discussions with Martha Withjack, Or Bialik, and Mark Deptuck were useful in clarifying aspects of the tectonic development of the Atlantic margin. In addition, the authors would like to extend special thanks to Lindsay Worthington, Vadim Levin, and Daniel Lizarralde for providing data. We thank Tom Pratt, USGS, for his thorough internal review and Maryline Moulin, Graeme Eagles, and an anonymous reviewer for their constructive comments. The analysis was carried out with Schlumberger's Petrel interpretation software under academic licenses to the University of Haifa and to Rutgers University. Use of trade, product, or firm names is for descriptive purposes only and does not imply endorsement by the U.S. government.

References

Abdelmalak, M. M., Faleide, J. I., Planke, S., Gernigon, L., Zastrozhnov, D., Shephard, G. E., & Myklebust, R. (2017). The T-reflection and the deep crustal structure of the Vøring Margin, offshore mid-Norway. *Tectonics*, *36*, 2497–2523. https://doi.org/10.1002/2017tc004617

Anderson, D. L. (1982). Hotspots, polar wander, Mesozoic convection and the geoid. *Nature*, *297*(5865), 391–393. https://doi.org/10.1038/297391a0

Anderson, D. L., Zhang, Y.-S., & Tanimoto, T. (1992). Plume heads, continental lithosphere, flood basalts and tomography. *Geological Society of London, Special Publication*, *68*(1), 99–124. https://doi.org/10.1144/gsl.sp.1992.068.01.07

Andrews, B. D., Chaytor, J. D., Uri, S., Brothers, D. S., Gardner, J. V., Lobecker, E. A., & Calder, B. R. (2013). Bathymetric terrain model of the Atlantic margin for marine geological investigations Rep. 2331-1258, US Geological Survey.

Austin, J. A., Stoffa, P. L., Phillips, J. D., Oh, J., Sawyer, D. S., Purdy, G. M., et al. (1990). Crustal structure of the Southeast Georgia embayment-Carolina trough: Preliminary results of a composite seismic image of a continental suture (?) and a volcanic passive margin. *Geology*, *18*(10), 1023–1027. https://doi.org/10.1130/0091-7613(1990)018%3c1023:csotsg%3e2.3.co;2

Autin, J., Bellahsen, N., Leroy, S., Husson, L., Beslier, M.-O., & D'Acremont, E. (2013). The role of structural inheritance in oblique rifting: Insights from analogue models and application to the Gulf of Aden. *Tectonophysics*, *607*, 51–64. https://doi.org/10.1016/j.tecto.2013.05.041

Bastow, I. D., & Keir, D. (2011). The protracted development of the continent–ocean transition in Afar. *Nature Geoscience*, *4*(4), 248–250. https://doi.org/10.1038/ngeo1095

Behn, M. D., & Lin, J. (2000). Segmentation in gravity and magnetic anomalies along the US East Coast passive margin: Implications for incipient structure of the oceanic lithosphere. *Journal of Geophysical Research*, *105*(B11), 25,769–25,790. https://doi.org/10.1029/2000JB900292

Bennett, S. E., & Oskin, M. E. (2014). Oblique rifting ruptures continents: Example from the Gulf of California shear zone. *Geology*, *42*(3), 215–218. https://doi.org/10.1130/g34904.1

Benson, R. N. (2003). *Age estimates of the seaward-dipping volcanic wedge, earliest oceanic crust, and earliest drift-stage sediments along the North American Atlantic continental margin, The Central Atlantic Magmatic Province: Insights From Fragments of Pangea* (Vol. 136, pp. 61–75). Washington, DC: Geophysical Union.

Benson, R. N., & Doyle, R. G. (1988). Early Mesozoic rift basins and the development of the United States middle Atlantic continental margin. In *Developments in Geotectonics* (pp. 99–127). Amsterdam: Elsevier.

Biari, Y., Klingelhoefer, F., Sahabi, M., Funck, T., Benabdellouahed, M., Schnabel, M., et al. (2017). Opening of the central Atlantic Ocean: Implications for geometric rifting and asymmetric initial seafloor spreading after continental breakup. *Tectonics*, *36*, 1129–1150. https://doi.org/10.1002/2017tc004596

Blaich, O. A., Faleide, J. I., & Tsikalas, F. (2011). Crustal breakup and continent-ocean transition at South Atlantic conjugate margins. *Journal of Geophysical Research*, *116*, B01402. https://doi.org/10.1029/2010jb007686

Brandl, P. A., Regelous, M., Beier, C., & Haase, K. M. (2013). High mantle temperatures following rifting caused by continental insulation. *Nature Geoscience*, *6*(5), 391–394. https://doi.org/10.1038/ngeo1758

Brune, S., Heine, C., Clift, P. D., & Pérez-Gussinyé, M. (2017). Rifted margin architecture and crustal rheology: Reviewing Iberia-Newfoundland, central South Atlantic, and South China Sea. *Marine and Petroleum Geology*, *79*, 257–281. https://doi.org/10.1016/j.marpetgeo.2016.10.018

Brune, S., Heine, C., Pérez-Gussinyé, M., & Sobolev, S. V. (2014). Rift migration explains continental margin asymmetry and crustal hyper-extension. *Nature Communications*, *5*, 4041. https://doi.org/10.1038/ncomms5014

Buck, W. R. (2004). Consequences of asthenospheric variability on continental rifting. In *Rheology and deformation of the lithosphere at continental margins* (Vol. 62, pp. 1–30). New York: Columbia University Press. https://doi.org/10.7312/karn12738-002

Buck, W. R. (2006). The role of magma in the development of the Afro-Arabian rift system. *Geological Society of London, Special Publication*, *259*(1), 43–54. https://doi.org/10.1144/gsl.sp.2006.259.01.05

Buck, W. R., Lavier, L. L., & Poliakov, A. N. (1999). How to make a rift wide. *Philosophical Transactions of the Royal Society of London, Series A: Mathematical, Physical and Engineering Sciences*, *357*(1753), 671–693. https://doi.org/10.1098/rsta.1999.0348

Buck, W. R., Martinez, F., Steckler, M. S., & Cochran, J. R. (1988). Thermal consequences of lithospheric extension: Pure and simple. *Tectonics*, *7*(2), 213–234. https://doi.org/10.1029/tc007i002p00213

Christensen, N. I., & Mooney, W. D. (1995). Seismic velocity structure and composition of the continental crust: A global view. *Journal of Geophysical Research*, *100*(B6), 9761–9788. https://doi.org/10.1029/95jb00259

Clerc, C., Jolivet, L., & Ringenbach, J.-C. (2015). Ductile extensional shear zones in the lower crust of a passive margin. *Earth and Planetary Science Letters*, *431*, 1–7. https://doi.org/10.1016/j.epsl.2015.08.038

Clerc, C., Ringenbach, J.-C., Jolivet, L., & Ballard, J.-F. (2018). Rifted margins: Ductile deformation, boudinage, continentward-dipping normal faults and the role of the weak lower crust. *Gondwana Research*, *53*, 20–40. https://doi.org/10.1016/j.gr.2017.04.030

Cook, F. A., & Vasudevan, K. (2006). Reprocessing and enhanced interpretation of the initial COCORP southern Appalachians traverse. *Tectonophysics*, *420*(1–2), 161–174. https://doi.org/10.1016/j.tecto.2006.01.022

Cousminer, H. L., & Steinkraus, W. E. (1988). Biostratigraphy of the COST G-2 well (Georges Bank): A record of Late Triassic synrift evaporite deposition; Liassic doming; and Mid-Jurassic to Miocene postrift marine sedimentation. In *Developments in Geotectonics* (pp. 167–184). Amsterdam: Elsevier.

Cumming, L., Gupta, N., Miller, K., Lombardi, C., Goldberg, D., Ten Brink, U., et al. (2017). Mid-Atlantic US offshore carbon storage resource assessment. *Energy Procedia*, *114*, 4629–4636. https://doi.org/10.1016/j.egypro.2017.03.1590

Dauteuil, O., & Brun, J. P. (1996). Deformation partitioning in a slow spreading ridge undergoing oblique extension: Mohns Ridge, Norwegian Sea. *Tectonics*, *15*(4), 870–884. https://doi.org/10.1029/95tc03682

Davis, J., Bécel, A., & Buck, W. (2018). Estimating emplacement rates for seaward-dipping reflectors associated with the US East Coast Magnetic Anomaly. *Geophysical Journal International*, *215*(3), 1594–1603. https://doi.org/10.1093/gji/ggy360

Davison, I. (1997). Wide and narrow margins of the Brazilian South Atlantic. *Journal of the Geological Society*, *154*(3), 471–476. https://doi.org/10.1144/gsjgs.154.3.0471

Dehler, S. A. (2012). Initial rifting and breakup between Nova Scotia and Morocco: Insight from new magnetic models. *Canadian Journal of Earth Sciences*, *49*(12), 1385–1394. https://doi.org/10.1139/e2012-073

Deptuck, M. (2020). Nova Scotia's volcanic passive margin-exploration history, geology, and play concepts off southwestern Nova Scotia Report, 32 pp, Canada-Nova Scotia Offshore Petroleum Board.

Deptuck, M., & Kendell, K. (2017). A review of Mesozoic-Cenozoic salt tectonics along the Scotian margin, eastern Canada. In *Permo-Triassic Salt Provinces of Europe, North Africa and the Atlantic Margins* (pp. 287–312). Amsterdam: Elsevier.

Doré, A., & Lundin, E. (2015). Research focus: Hyperextended continental margins—Knowns and unknowns. *Geology*, *43*(1), 95–96. https://doi.org/10.1130/focus012015.1

Doré, A., Lundin, E., Jensen, L., Birkeland, Ø., Eliassen, P., & Fichler, C. (1999). Principal tectonic events in the evolution of the northwest European Atlantic margin, Paper presented at Geological Society, London, Petroleum Geology Conference Series, Geological Society of London.

Dunbar, J. A., & Sawyer, D. S. (1989). How preexisting weaknesses control the style of continental breakup. *Journal of Geophysical Research*, *94*(B6), 7278–7292. https://doi.org/10.1029/jb094ib06p07278

Eagles, G., Pérez-Díaz, L., & Scarselli, N. (2015). Getting over continent ocean boundaries. *Earth-Science Reviews*, *151*, 244–265. https://doi.org/10.1016/j.earscirev.2015.10.009

Ebinger, C., & Casey, M. (2001). Continental breakup in magmatic provinces: An Ethiopian example. *Geology*, *29*(6), 527–530. https://doi.org/10.1130/0091-7613(2001)029%3c0527:cbimpa%3e2.0.co;2

Eldholm, O., Gladczenko, T., Skogseid, J., & Planke, S. (2000). Atlantic volcanic margins: A comparative study. *Geological Society of London, Special Publication*, *167*(1), 411–428. https://doi.org/10.1144/gsl.sp.2000.167.01.16

Eldholm, O., Skogseid, J., Planke, S., & Gladczenko, T. (1995). Volcanic margin concepts. In *Rifted Ocean-Continent Boundaries* (pp. 1–16). Dordrecht: Springer.

Elkins, L. J., Meyzen, C. M., Callegaro, S., Marzoli, A., & Bizimis, M. (2020). Assessing origins of end-Triassic tholeiites from Eastern North America using hafnium isotopes. *Geochemistry, Geophysics, Geosystems*, *21*, e2020GC008999. https://doi.org/10.1029/2020gc008999

Elkins-Tanton, L. T. (2007). Continental magmatism, volatile recycling, and a heterogeneous mantle caused by lithospheric gravitational instabilities. *Journal of Geophysical Research*, *112*, B03405. https://doi.org/10.1029/2005jb004072

Falvey, D. A. (1974). The development of continental margins in plate tectonic theory. *The APPEA Journal*, *14*(1), 95–106. https://doi.org/10.1071/aj73012

Fazlikhani, H., Fossen, H., Gawthorpe, R. L., Faleide, J. I., & Bell, R. E. (2017). Basement structure and its influence on the structural configuration of the northern North Sea rift. *Tectonics*, *36*, 1151–1177. https://doi.org/10.1002/2017tc004514

Fortin, W., Goldberg, D., & Slagle, A. (2018). Potential for CO_2 sequestration in rift basins offshore the US East Coast: Updated basin extent and composition from prestack seismic inversion, Paper presented at AGU Fall Meeting Abstracts.

Franke, D. (2013). Rifting, lithosphere breakup and volcanism: Comparison of magma-poor and volcanic rifted margins. *Marine and Petroleum Geology*, *43*, 63–87. https://doi.org/10.1016/j.marpetgeo.2012.11.003

Franke, D., Neben, S., Ladage, S., Schreckenberger, B., & Hinz, K. (2007). Margin segmentation and volcano-tectonic architecture along the volcanic margin off Argentina/Uruguay, South Atlantic. *Marine Geology*, *244*(1–4), 46–67. https://doi.org/10.1016/j.margeo.2007.06.009

Funck, T., Jackson, H. R., Louden, K. E., Dehler, S. A., & Wu, Y. (2004). Crustal structure of the northern Nova Scotia rifted continental margin (eastern Canada). *Journal of Geophysical Research*, *109*, B09102. https://doi.org/10.1029/2004JB003008

Geoffroy, L. (2005). Volcanic passive margins. *Comptes Rendus Geoscience*, *337*(16), 1395–1408. https://doi.org/10.1016/j.crte.2005.10.006

Geoffroy, L., Burov, E., & Werner, P. (2015). Volcanic passive margins: Another way to break up continents. *Scientific Reports*, *5*, 14828. https://doi.org/10.1038/srep14828

Greene, J. A., Tominaga, M., Miller, N. C., Hutchinson, D. R., & Karl, M. R. (2017). Refining the formation and early evolution of the eastern North American margin: New insights from multiscale magnetic anomaly analyses. *Journal of Geophysical Research: Solid Earth*, *122*, 8724–8748. https://doi.org/10.1002/2017JB014308

Guan, H., Geoffroy, L., Gernigon, L., Chauvet, F., Grigné, C., & Werner, P. (2019). Magmatic ocean-continent transitions. *Marine and Petroleum Geology*, *104*, 438–450. https://doi.org/10.1016/j.marpetgeo.2019.04.003

Hames, W., Renne, P., & Ruppel, C. (2000). New evidence for geologically instantaneous emplacement of earliest Jurassic Central Atlantic magmatic province basalts on the North American margin. *Geology*, *28*(9), 859–862. https://doi.org/10.1130/0091-7613(2000)028%3c0859:nefgie%3e2.3.co;2

Harry, D. L., & Sawyer, D. S. (1992). A dynamic model of extension in the Baltimore Canyon Trough region. *Tectonics*, *11*(2), 420–436. https://doi.org/10.1029/91tc03012

Hatcher, R. D., Tollo, R., Bartholomew, M., Hibbard, J., & Karabinos, P. (2010). *The Appalachian orogen: A brief summary, From Rodinia to Pangea: The Lithotectonic record of the Appalachian region*, *Memoir* (Vol. 206, pp. 1–19). Boulder, CO: Geological Society of America.

Hibbard, J., Van Staal, C., Ranki, D., & Williams, H. (2006). Lithotectonic map of the Appalachian orogen, Canada–United States of America, geological survey of Canada, map A, 2096, 2.

Hibbard, J. P., van Staal, C. R., & Miller, B. V. (2007). *Links among Carolinia, Avalonia, and Ganderia in the Appalachian peri-Gondwanan realm*, *Special Papers* (Vol. 433, pp. 291–311). Boulder, CO: Geological Society of America.

Hibbard, J. P., van Staal, C. R., Rankin, D. W., Tollo, R., & Bartholomew, M. (2010). *Comparative analysis of the geological evolution of the northern and southern Appalachian orogen: Late Ordovician-Permian, From Rodinia to Pangea: The Lithotectonic Record of the Appalachian Region*, *Memoir* (Vol. 206, pp. 51–69). Boulder, CO: Geological Society of America.

Hinz, K. (1981). A hypothesis on terrestrial catastrophes Wedges of very thick oceanward dipping layers beneath passive continental margins—Their origin and paleoenvironmental significance. *Geologiches Jahrbuch*, *22*, 345–363.

Holbrook, W. S., & Kelemen, P. (1993). Large igneous province on the US Atlantic margin and implications for magmatism during continental breakup. *Nature*, *364*(6436), 433. https://doi.org/10.1038/364433a0

Holbrook, W. S., Purdy, G., Collins, J., Sheridan, R., Musser, D., Glover, L. III, et al. (1992). Deep velocity structure of rifted continental crust, US mid-Atlantic Margin, from wide-angle reflection/refraction data. *Geophysical Research Letters*, *19*(16), 1699–1702. https://doi.org/10.1029/92gl01799

Holbrook, W. S., Purdy, G., Sheridan, R., Glover, L., Talwani, M., Ewing, J., & Hutchinson, D. (1994). Seismic structure of the US mid-Atlantic continental margin. *Journal of Geophysical Research*, *99*(B9), 17,871–17,891. https://doi.org/10.1029/94JB00729

Hole, M. J. (2015). The generation of continental flood basalts by decompression melting of internally heated mantle. *Geology*, *43*(4), 311–314. https://doi.org/10.1130/g36442.1

Hopper, J. R., Dahl-Jensen, T., Holbrook, W. S., Larsen, H. C., Lizarralde, D., Korenaga, J., et al. (2003). Structure of the SE Greenland margin from seismic reflection and refraction data: Implications for nascent spreading center subsidence and asymmetric crustal accretion during North Atlantic opening. *Journal of Geophysical Research*, *108*(B5), 2269. https://doi.org/10.1029/2002JB001996

Hopper, J. R., Mutter, J. C., Larson, R. L., & Mutter, C. Z. (1992). Magmatism and rift margin evolution: Evidence from Northwest Australia. *Geology*, *20*(9), 853–857. https://doi.org/10.1130/0091-7613(1992)020%3c0853:marmee%3e2.3.co;2

Hughes, S., & Luetgert, J. H. (1991). Crustal structure of the western New England Appalachians and the Adirondack mountains. *Journal of Geophysical Research*, *96*(B10), 16,471–16,494. https://doi.org/10.1029/91JB01657

Huismans, R., & Beaumont, C. (2011). Depth-dependent extension, two-stage breakup and cratonic underplating at rifted margins. *Nature*, *473*(7345), 74–78. https://doi.org/10.1038/nature09988

Huismans, R. S., & Beaumont, C. (2014). Rifted continental margins: The case for depth-dependent extension. *Earth and Planetary Science Letters*, *407*, 148–162. https://doi.org/10.1016/j.epsl.2014.09.032

Hutchinson, D., & Klitgord, K. (1988). Evolution of rift basins on the continental margin off southern New England. In *Developments in Geotectonics* (pp. 81–98). Amsterdam: Elsevier.

Hutchinson, D., Klitgord, K., & Detrick, R. (1985). Block Island fault: A Paleozoic crustal boundary on the Long Island platform. *Geology*, *13*(12), 875–879. https://doi.org/10.1130/0091-7613(1985)13%3c875:bifapc%3e2.0.co;2

Hutchinson, D., Klitgord, K., & Detrick, R. (1986). Rift basins of the Long Island platform. *Geological Society of America Bulletin*, *97*(6), 688–702. https://doi.org/10.1130/0016-7606(1986)97%3c688:rbotli%3e2.0.co;2

Hutchinson, D., Klitgord, K., Lee, M., & Tréhu, A. (1988). US geological survey deep seismic reflection profile across the Gulf of Maine. *Geological Society of America Bulletin*, *100*(2), 172–184. https://doi.org/10.1130/0016-7606(1988)100%3c0172:usgsds%3e2.3.co;2

Hutchinson, D., Klitgord, K., & Tréhu, A. (1987). Structure of the lower crust beneath the Gulf of Maine. *Geophysical Journal of the Royal Astronomical Society*, *89*(1), 189–194. https://doi.org/10.1111/j.1365-246x.1987.tb04407.x

Jordan, L. M. (2019). Quantitative biostratigraphic analysis of middle Cretaceous sequences in the Baltimore Canyon Trough offshore mid-Atlantic US margin, Rutgers The State University of New Jersey, School of Graduate Studies.

Keen, C., Kay, W., Keppie, D., Marillier, F., Pe-Piper, G., & Waldron, J. (1991). Deep seismic reflection data from the Bay of Fundy and Gulf of Maine: Tectonic implications for the northern Appalachians. *Canadian Journal of Earth Sciences*, *28*(7), 1096–1111. https://doi.org/10.1139/e91-099

Keen, C., & Potter, D. (1995). The transition from a volcanic to a nonvolcanic rifted margin off eastern Canada. *Tectonics*, *14*(2), 359–371. https://doi.org/10.1029/94tc03090

Keir, D., Ebinger, C., Stuart, G., Daly, E., & Ayele, A. (2006). Strain accommodation by magmatism and faulting as rifting proceeds to breakup: Seismicity of the northern Ethiopian rift. *Journal of Geophysical Research*, *111*, B05314. https://doi.org/10.1029/2005jb003748

Kelemen, P. B., & Holbrook, W. S. (1995). Origin of thick, high-velocity igneous crust along the US East Coast Margin. *Journal of Geophysical Research*, *100*(B6), 10,077–10,094. https://doi.org/10.1029/95JB00924

Kendall, J.-M., Stuart, G., Ebinger, C., Bastow, I., & Keir, D. (2005). Magma-assisted rifting in Ethiopia. *Nature*, *433*(7022), 146. https://doi.org/10.1038/nature03161

King, S. D., & Anderson, D. L. (1998). Edge-driven convection. *Earth and Planetary Science Letters*, *160*(3–4), 289–296. https://doi.org/10.1016/s0012-821x(98)00089-2

Klingelhoefer, F., Biari, Y., Sahabi, M., Aslanian, D., Schnabel, M., Matias, L., et al. (2016). Crustal structure variations along the NW-African continental margin: A comparison of new and existing models from wide-angle and reflection seismic data. *Tectonophysics*, *674*, 227–252. https://doi.org/10.1016/j.tecto.2016.02.024

Klitgord, K. D., & Behrendt, J. C. (1979). Basin Structure of the U.S. Atlantic Margin: Rifted Margins. In *Geological and Geophysical Investigations of Continental Margins* (pp. 85–112). Boulder, CO: Geol. Soc. Am.

Klitgord, K. D., Hutchinson, D. R., & Schouten, H. (1988). *US Atlantic continental margin; structural and tectonic framework*, *The Geology of North America* (Vol. 2, pp. 19–55). Boulder, CO: Geological Society of America.

Klitgord, K. D., Poag, C., Schneider, C., & North, L. (1994). Geophysical database of the East Coast of the United States northern Atlantic margin-cross sections and gridded database (Georges Bank Basin, Long Island Platform, and Baltimore Canyon Trough) Rep. 2331–1258.

Klitgord, K. D., Schlee, J. S., & Hinz, K. (1982). Basement structure, sedimentation and tectonic history of the Georges Bank Basin, Geological. Studies of the COST nos. G-1 and G-2 wells, US North Atlantic Outer Continental Shelf.

Klitgord, K. D., & Schouten, H. (1986). Plate kinematics of the central Atlantic. In B. E. Tucholke & P. R. Vogt (Eds.), *The Western North Atlantic Region*, *The Geology of North America* (Vol. M, pp. 351–378). Boulder, CO: Geological Society of America.

Kneller, E. A., Johnson, C. A., Karner, G. D., Einhorn, J., & Queffelec, T. A. (2012). Inverse methods for modeling non-rigid plate kinematics: Application to mesozoic plate reconstructions of the Central Atlantic. *Computers & Geosciences*, *49*, 217–230.

Kuiper, Y. D., Thompson, M. D., Barr, S. M., White, C. E., Hepburn, J. C., & Crowley, J. L. (2017). Detrital zircon evidence for Paleoproterozoic West African crust along the eastern North American continental margin, Georges Bank, offshore Massachusetts, USA. *Geology*, *45*(9), 811–814. https://doi.org/10.1130/g39203.1

Labails, C., Olivet, J.-L., Aslanian, D., & Roest, W. R. (2010). An alternative early opening scenario for the Central Atlantic Ocean. *Earth and Planetary Science Letters*, *297*(3–4), 355–368. https://doi.org/10.1016/j.epsl.2010.06.024

Labails, C., Olivet, J.-L., & Group, D. S. (2009). Crustal structure of the SW Moroccan margin from wide-angle and reflection seismic data (the Dakhla experiment) Part B—The tectonic heritage. *Tectonophysics*, *468*(1–4), 83–97. https://doi.org/10.1016/j.tecto.2008.08.028

LASE (1986). Deep structure of the US East Coast passive margin from large aperture seismic experiments (LASE). *Marine and Petroleum Geology*, *3*(3), 234–242. https://doi.org/10.1016/0264-8172(86)90047-4

Latin, D., & White, N. (1990). Generating melt during lithospheric extension: Pure shear vs. simple shear. *Geology*, *18*(4), 327–331. https://doi.org/10.1130/0091-7613(1990)018%3c0327:gmdlep%3e2.3.co;2

Lavier, L. L., & Manatschal, G. (2006). A mechanism to thin the continental lithosphere at magma-poor margins. *Nature*, *440*(7082), 324. https://doi.org/10.1038/nature04608

Le Pichon, X., & Fox, P. J. (1971). Marginal offsets, fracture zones, and the early opening of the North Atlantic. *Journal of Geophysical Research*, *76*(26), 6294–6308. https://doi.org/10.1029/JB076i026p06294

Le Roy, P., & Piqué, A. (2001). Triassic–Liassic Western Moroccan synrift basins in relation to the Central Atlantic opening. *Marine Geology*, *172*(3–4), 359–381. https://doi.org/10.1016/s0025-3227(00)00130-4

Leleu, S., & Hartley, A. J. (2010). Controls on the stratigraphic development of the Triassic Fundy Basin, Nova Scotia: Implications for the tectonostratigraphic evolution of Triassic Atlantic rift basins. *Journal of the Geological Society*, *167*(3), 437–454. https://doi.org/10.1144/0016-76492009-092

Leleu, S., Hartley, A. J., van Oosterhout, C., Kennan, L., Ruckwied, K., & Gerdes, K. (2016). Structural, stratigraphic and sedimentological characterisation of a wide rift system: The Triassic rift system of the Central Atlantic Domain. *Earth-Science Reviews*, *158*, 89–124. https://doi.org/10.1016/j.earscirev.2016.03.008

Li, C., Gao, H., Williams, M. L., & Levin, V. (2018). Crustal thickness variation in the northern Appalachian Mountains: Implications for the geometry of 3D tectonic Bboundaries within the crust. *Geophysical Research Letters*, *45*, 6061–6070. https://doi.org/10.1029/2018gl078777

Lister, G., Etheridge, M., & Symonds, P. (1991). Detachment models for the formation of passive continental margins. *Tectonics*, *10*(5), 1038–1064. https://doi.org/10.1029/90tc01007

Lizarralde, D., & Holbrook, W. S. (1997). US mid-Atlantic margin structure and early thermal evolution. *Journal of Geophysical Research*, *102*(B10), 22,855–22,875. https://doi.org/10.1029/96JB03805

Luckie, T., Worthington, L. L., & Magnani, M. B. (2016). Relationship between magmatism and extension along the Eastern North American Margin (ENAM) from onshore-offshore active source ENAM community seismic experiment refraction data. *AGU Fall Meeting*.

Lundin, E. R., Redfield, T. F., Péron-Pindivic, G., & Pindell, J. (2014). Rifted continental margins: Geometric influence on crustal architecture and melting, Paper presented at 33rd annual GCSSEPM foundation Bob F. Perkins conference. Sedimentary Basins: Origin, Depositional Histories, and Petroleum Systems. Gulf Coast Section SEPM, Houston, TX.

Maillard, A., Malod, J., Thiébot, E., Klingelhoefer, F., & Réhault, J.-P. (2006). Imaging a lithospheric detachment at the continent–ocean crustal transition off Morocco. *Earth and Planetary Science Letters*, *241*(3–4), 686–698. https://doi.org/10.1016/j.epsl.2005.11.013

Manatschal, G. (2004). New models for evolution of magma-poor rifted margins based on a review of data and concepts from West Iberia and the Alps. *International Journal of Earth Sciences*, *93*(3), 432–466. https://doi.org/10.1007/s00531-004-0394-7

Manatschal, G., Lavier, L., & Chenin, P. (2015). The role of inheritance in structuring hyperextended rift systems: Some considerations based on observations and numerical modeling. *Gondwana Research*, *27*(1), 140–164. https://doi.org/10.1016/j.gr.2014.08.006

Marillier, F., Keen, C. E., Stockmal, G. S., Quinlan, G., Williams, H., Colman-Sadd, S. P., & O'Brien, S. J. (1989). Crustal structure and surface zonation of the Canadian Appalachians: Implications of deep seismic reflection data. *Canadian Journal of Earth Sciences*, *26*(2), 305–321. https://doi.org/10.1139/e89-025

Marzen, R. E., Shillington, D. J., Lizarralde, D., & Harder, S. H. (2019). Constraints on Appalachian orogenesis and continental rifting in the southeastern United States from wide-angle seismic data. *Journal of Geophysical Research: Solid Earth*, *124*, 6625–6652. https://doi.org/10.1029/2019JB017611

Marzoli, A., Callegaro, S., Dal Corso, J., Davies, J. H., Chiaradia, M., Youbi, N., et al. (2018). The central Atlantic magmatic province (CAMP): A review. In *The Late Triassic World* (pp. 91–125). Cham: Springer.

Marzoli, A., Jourdan, F., Puffer, J. H., Cuppone, T., Tanner, L. H., Weems, R. E., et al. (2011). Timing and duration of the Central Atlantic magmatic province in the Newark and Culpeper basins, eastern USA. *Lithos*, *122*(3–4), 175–188. https://doi.org/10.1016/j.lithos.2010.12.013

Marzoli, A., Renne, P. R., Piccirillo, E. M., Ernesto, M., Bellieni, G., & De Min, A. (1999). Extensive 200-million-year-old continental flood basalts of the central Atlantic magmatic province. *Science*, *284*(5414), 616–618. https://doi.org/10.1126/science.284.5414.616

McBride, J., & Nelson, K. (1988). Integration of COCORP deep reflection and magnetic anomaly analysis in the southeastern United States: Implications for origin of the Brunswick and East Coast magnetic anomalies. *Geological Society of America Bulletin*, *100*(3), 436–445. https://doi.org/10.1130/0016-7606(1988)100%3c0436:iocdra%3e2.3.co;2

McHone, J. G. (2000). Non-plume magmatism and rifting during the opening of the central Atlantic Ocean. *Tectonophysics*, *316*(3–4), 287–296. https://doi.org/10.1016/s0040-1951(99)00260-7

McKenzie, D. (1978). Some remarks on the development of sedimentary basins. *Earth and Planetary Science Letters*, *40*(1), 25–32. https://doi.org/10.1016/0012-821x(78)90071-7

Menzies, M. A., Klemperer, S. L., Ebinger, C. J., & Baker, J. (2002). Characteristics of volcanic rifted margins. In *Volcanic rifted margins*, *Special Papers* (Vol. 362, pp. 1–14). Boulder, CO: Geological Society of America.

Mercier de Lépinay, M., Loncke, L., Basile, C., Roest, W. R., Patriat, M., Maillard, A., & De Clarens, P. (2016). Transform continental margins—Part 2: A worldwide review. *Tectonophysics*, *693*, 96–115. https://doi.org/10.1016/j.tecto.2016.05.038

Meyer, B., Saltus, R., & Chulliat, A. (2017). EMAG2: Earth magnetic anomaly grid (2-arc-minute resolution) version 3, National Centers for Environmental Information, NOAA. Model. doi, 10, V5H70CVX.

Miller, K. G., Lombardi, C. J., Browning, J. V., Schmelz, W. J., Gallegos, G., Mountain, G. S., & Baldwin, K. E. (2018). Back to basics of sequence stratigraphy: Early Miocene and mid-Cretaceous examples from the New Jersey paleoshelf. *Journal of Sedimentary Research*, *88*(1), 148–176. https://doi.org/10.2110/jsr.2017.73

Misra, A. A., & Mukherjee, S. (2015). *Tectonic inheritance in continental rifts and passive margins*. Cham: Springer.

Mitchum Jr., R., Vail, P., & Thompson III, S. (1977). Seismic stratigraphy and global changes of sea level: Part 2. The depositional sequence as a basic unit for stratigraphic analysis: Section 2. Application of seismic reflection configuration to stratigraphic interpretation.

Morley, C., Nelson, R., Patton, T., & Munn, S. (1990). Transfer zones in the East African rift system and their relevance to hydrocarbon exploration in rifts (1). *AAPG Bulletin*, *74*(8), 1234–1253. https://doi.org/10.1306/0c9b2475-1710-11d7-8645000102c1865d

Mutter, J. C., Buck, W. R., & Zehnder, C. M. (1988). Convective partial melting: 1. A model for the formation of thick basaltic sequences during the initiation of spreading. *Journal of Geophysical Research*, *93*(B2), 1031–1048. https://doi.org/10.1029/JB093ib02p01031

Mutter, J. C., Talwani, M., & Stoffa, P. L. (1982). Origin of seaward-dipping reflectors in oceanic crust off the Norwegian margin by "subaerial sea-floor spreading". *Geology*, *10*(7), 353–357. https://doi.org/10.1130/0091-7613(1982)10%3c353:oosrio%3e2.0.co;2

Nomade, S., Knight, K., Beutel, E., Renne, P., Verati, C., Féraud, G., et al. (2007). Chronology of the Central Atlantic Magmatic Province: Implications for the Central Atlantic rifting processes and the Triassic–Jurassic biotic crisis. *Palaeogeography Palaeoclimatology Palaeoecology*, *244*(1–4), 326–344. https://doi.org/10.1016/j.palaeo.2006.06.034

O'Brien, S., O'Brien, B., Dunning, G., & Tucker, R. (1996). Late Neoproterozoic Avalonian and related peri-Gondwanan rocks of the Newfoundland Appalachians. *Avalonian and related peri-Gondwanan terranes of the Circum-North Atlantic*, *Special Papers* (Vol. 304, pp. 9–28). Boulder, Co: Geological Society of America.

Olsen, P. E. (1997). Stratigraphic record of the early Mesozoic breakup of Pangea in the Laurasia-Gondwana rift system. *Annual Review of Earth and Planetary Sciences*, *25*(1), 337–401. https://doi.org/10.1146/annurev.earth.25.1.337

Olsen, P. E. (1999). Giant lava flows, mass extinctions, and mantle plumes. *Science*, *284*(5414), 604–605. https://doi.org/10.1126/science.284.5414.604

Olsen, P. E., Kent, D. V., Et-Touhami, M., & Puffer, J. (2003). Cyclo-, magneto-, and bio-stratigraphic constraints on the duration of the CAMP event and its relationship to the Triassic-Jurassic boundary.

Paton, D., Pindell, J., McDermott, K., Bellingham, P., & Horn, B. (2017). Evolution of seaward-dipping reflectors at the onset of oceanic crust formation at volcanic passive margins: Insights from the South Atlantic. *Geology*, *45*(5), 439–442. https://doi.org/10.1130/g38706.1

Pe Piper, G., & Jansa, L. (1999). Pre-Mesozoic basement rocks offshore Nova Scotia, Canada: New constraints on the accretion history of the Meguma terrane. *Geological Society of America Bulletin*, *111*(12), 1773–1791. https://doi.org/10.1130/0016-7606(1999)111%3c1773:pmbron%3e2.3.co;2

Peron-Pinvidic, G., Manatschal, G., & Osmundsen, P. T. (2013). Structural comparison of archetypal Atlantic rifted margins: A review of observations and concepts. *Marine and Petroleum Geology*, *43*, 21–47. https://doi.org/10.1016/j.marpetgeo.2013.02.002

Phillips, T. B., Jackson, C. A., Bell, R. E., Duffy, O. B., & Fossen, H. (2016). Reactivation of intrabasement structures during rifting: A case study from offshore southern Norway. *Journal of Structural Geology*, *91*, 54–73. https://doi.org/10.1016/j.jsg.2016.08.008

Planke, S., Symonds, P. A., Alvestad, E., & Skogseid, J. (2000). Seismic volcanostratigraphy of large-volume basaltic extrusive complexes on rifted margins. *Journal of Geophysical Research*, *105*(B8), 19,335–19,351. https://doi.org/10.1029/1999JB900005

Poag, C. W. (1985). *Depositional history and stratigraphic reference section for central Baltimore Canyon Trough, Geologic Evolution of the United States Atlantic Margin* (pp. 217–263). New York: Van Nostrand Reinhold.

Poag, C. W. (1991). Rise and demise of the Bahama-Grand Banks gigaplatform, northern margin of the Jurassic proto-Atlantic seaway. *Marine Geology*, *102*(1–4), 63–130. https://doi.org/10.1016/0025-3227(91)90006-p

Poag, C. W., & Sevon, W. D. (1989). A record of Appalachian denudation in postrift Mesozoic and Cenozoic sedimentary deposits of the US middle Atlantic continental margin. *Geomorphology*, *2*(1–3), 119–157. https://doi.org/10.1016/0169-555x(89)90009-3

Poag, C. W., & Valentine, C. P. (1988). Mesozoic and Cenozoic stratigraphy of the United States Atlantic continental shelf and slope. In R. E. Sheridan & J. A. Grow (Eds.), *The Atlantic Continental Margin*, *The Geology of North America* (Vol. 1–2, pp. 67–85). Boulder, CO: The Geological Society of America.

Pope, J. P., Andreasen, D. C., Mcfarland, E. R., & Watt, M. K. (2016). Digital elevations and extents of regional hydrogeologic units in the Northern Atlantic Coastal Plain aquifer system from Long Island, New York, to North Carolina rep. 2327-638X, US Geological Survey.

Poppe, L., Poag, C., & Stanton, R. (1992a). Lithology, stratigraphy, and paleoenvironments of the Mobil 312-1 well, Georges Bank Basin, US North Atlantic outer continental shelf. *Northeastern Geology*, *14*, 156–170.

Poppe, L., Poag, C., & Stanton, R. (1992b). Mid-Mesozoic (mid-Jurassic to Early Cretaceous) evolution of the Georges Bank Basin, US North Atlantic outer continental shelf: Sedimentology of the Conoco 145-1 well. *Sedimentary Geology*, *75*(3–4), 171–192. https://doi.org/10.1016/0037-0738(92)90091-5

Pratt, T. L., Çoruh, C., Costain, J. K., & Glover, L. III (1988). A geophysical study of the Earth's crust in central Virginia: Implications for Appalachian crustal structure. *Journal of Geophysical Research*, *93*(B6), 6649–6667. https://doi.org/10.1029/JB093ib06p06649

Reston, T. (2009). The structure, evolution and symmetry of the magma-poor rifted margins of the north and Central Atlantic: A synthesis. *Tectonophysics*, *468*(1–4), 6–27. https://doi.org/10.1016/j.tecto.2008.09.002

Reston, T., Krawczyk, C., & Klaeschen, D. (1996). The S reflector west of Galicia (Spain): Evidence from prestack depth migration for detachment faulting during continental breakup. *Journal of Geophysical Research*, *101*(B4), 8075–8091. https://doi.org/10.1029/95JB03466

Roberts, D., Thompson, M., Mitchener, B., Hossack, J., Carmichael, S., & Bjørnseth, H.-M. (1999). Palaeozoic to tertiary rift and basin dynamics: Mid-Norway to the Bay of Biscay—A new context for hydrocarbon prospectivity in the deep water frontier, Paper presented at geological society, London, petroleum geology conference series, Geological Society of London.

Ruiz-Martínez, V. C., Torsvik, T. H., van Hinsbergen, D. J., & Gaina, C. (2012). Earth at 200 Ma: Global paleogeography refined from CAMP palaeomagnetic data. *Earth and Planetary Science Letters*, *331*, 67–79. https://doi.org/10.1016/j.epsl.2012.03.008

Sahabi, M., Aslanian, D., & Olivet, J.-L. (2004). A new starting point for the history of the Central Atlantic. *Comptes Rendus Geoscience*, *336*(12), 1041–1052. https://doi.org/10.1016/j.crte.2004.03.017

Savva, D., Chrest, T., Saint-Ange, F., MacDonald, A., Luheshi, M., & Cuilhe, L. (2016) Structural impact of the Yarmouth Arch in the central Atlantic opening and on the SW Nova Scotian margin architecture (SW Nova Scotia 2011 PFA expansion), Paper presented at AAPG annual convention and exhibition.

Sawyer, D. S. (1985). Total tectonic subsidence: A parameter for distinguishing crust type at the US Atlantic continental margin. *Journal of Geophysical Research*, *90*(B9), 7751–7769. https://doi.org/10.1029/JB090ib09p07751

Sawyer, D. S., & Harry, D. L. (1991). Dynamic modeling of divergent margin formation: Application to the US Atlantic margin. *Marine Geology*, *102*(1–4), 29–42. https://doi.org/10.1016/0025-3227(91)90004-n

Schettino, A., & Turco, E. (2009). Breakup of Pangaea and plate kinematics of the Central Atlantic and atlas regions. *Geophysical Journal International*, *178*(2), 1078–1097. https://doi.org/10.1111/j.1365-246x.2009.04186.x

Schlee, J., & Fritsch, J. (1982). Seismic stratigraphy of the Georges Bank Basin complex offshore New England. *American Association of Petroleum Geologists Memoir*, *43*, 223–251.

Schlische, R. W. (1992). Structural and stratigraphic development of the Newark extensional basin, eastern North America: Evidence for the growth of the basin and its bounding structures. *Geological Society of America Bulletin*, *104*(10), 1246–1263. https://doi.org/10.1130/0016-7606(1992)104%3c1246:sasdot%3e2.3.co;2

Schlische, R. W., & Withjack, M. O. (2009). Origin of fault domains and fault-domain boundaries (transfer zones and accommodation zones) in extensional provinces: Result of random nucleation and self-organized fault growth. *Journal of Structural Geology*, *31*(9), 910–925. https://doi.org/10.1016/j.jsg.2008.09.005

Schmelz, W. J., Miller, K. G., Mountain, G. S., Browning, J. V., & Baldwin, K. E. (2019). Onshore-offshore correlations of Cretaceous fluvial-deltaic sequences, southern Baltimore Canyon trough. *AAPG Bulletin*, *104*, 411–448. https://doi.org/10.1306/05061918197

Schnabel, M., Franke, D., Engels, M., Hinz, K., Neben, S., Damm, V., et al. (2008). The structure of the lower crust at the argentine continental margin, South Atlantic at 44 S. *Tectonophysics*, *454*(1–4), 14–22. https://doi.org/10.1016/j.tecto.2008.01.019

Schreckenberger, B., Hinz, K., Franke, D., Neben, S., & Roeser, H. (2002). Marine magnetic anomalies and the symmetry of the conjugated rifted margins of the South Atlantic, paper presented at AGU Fall Meeting Abstracts.

Shellnutt, J. G., Dostal, J., & Yeh, M.-W. (2018). Mantle source heterogeneity of the early Jurassic basalt of eastern North America. *International Journal of Earth Sciences*, *107*(3), 1033–1058. https://doi.org/10.1007/s00531-017-1519-0

Sheridan, R. E., Maguire, T. J., Feigenson, M. D., Patino, L. C., & Volkert, R. A. (1999). Grenville age of basement rocks in Cape May NJ well: New evidence for Laurentian crust in US Atlantic coastal plain basement Chesapeake terrane. *Journal of Geodynamics*, *27*(4–5), 623–633. https://doi.org/10.1016/s0264-3707(98)00015-5

Sheridan, R. E., Musser, D. L., Glover, L. III, Talwani, M., Ewing, J. I., Holbrook, W. S., et al. (1993). Deep seismic reflection data of EDGE US mid-Atlantic continental-margin experiment: Implications for Appalachian sutures and Mesozoic rifting and magmatic underplating. *Geology*, *21*(6), 563–567. https://doi.org/10.1130/0091-7613(1993)021%3c0563:dsrdoe%3e2.3.co;2

Shuck, B. D., Van Avendonk, H. J., & Bécel, A. (2019). The role of mantle melts in the transition from rifting to seafloor spreading offshore eastern North America. *Earth and Planetary Science Letters*, *525*, 115756. https://doi.org/10.1016/j.epsl.2019.115756

Sibuet, J.-C., Maze, J.-P., Amortila, P., & Le Pichon, X. (1987). Physiography and structure of the western Iberian continental margin off Galicia from sea-beam and seismic data. In *Initial reports of the Ocean Drilling Program, part A* (Vol. 103, pp. 77–97). College Station, TX: Ocean Drilling Program.

Sibuet, J.-C., Rouzo, S., & Srivastava, S. (2012). Plate tectonic reconstructions and paleogeographic maps of the central and North Atlantic oceans. *Canadian Journal of Earth Sciences*, *49*(12), 1395–1415. https://doi.org/10.1139/e2012-071

Simon, K., Huismans, R. S., & Beaumont, C. (2009). Dynamical modelling of lithospheric extension and small-scale convection: Implications for magmatism during the formation of volcanic rifted margins. *Geophysical Journal International*, *176*(1), 327–350. https://doi.org/10.1111/j.1365-246x.2008.03891.x

Smith, M., Amato, R., Furbush, M., Pert, D., Nelson, M., Hendrix, J., et al. (1976). Geological and operational summary, COST no. B-2 well, Baltimore canyon trough area, mid-Atlantic OCS rep. 2331–1258, US Geological Survey.

Stab, M., Bellahsen, N., Pik, R., Quidelleur, X., Ayalew, D., & Leroy, S. (2016). Modes of rifting in magma-rich settings: Tectono-magmatic evolution of Central Afar. *Tectonics*, *35*, 2–38. https://doi.org/10.1002/2015tc003893

Steckler, M., & Watts, A. (1978). Subsidence of the Atlantic-type continental margin off New York. *Earth and Planetary Science Letters*, *41*(1), 1–13. https://doi.org/10.1016/0012-821x(78)90036-5

Stica, J. M., Zalán, P. V., & Ferrari, A. L. (2014). The evolution of rifting on the volcanic margin of the Pelotas Basin and the contextualization of the Paraná–Etendeka LIP in the separation of Gondwana in the South Atlantic. *Marine and Petroleum Geology*, *50*, 1–21. https://doi.org/10.1016/j.marpetgeo.2013.10.015

Sutra, E., Manatschal, G., Mohn, G., & Unternehr, P. (2013). Quantification and restoration of extensional deformation along the Western Iberia and Newfoundland rifted margins. *Geochemistry, Geophysics, Geosystems*, *14*, 2575–2597. https://doi.org/10.1002/ggge.20135

Svartman Dias, A. E., Lavier, L. L., & Hayman, N. W. (2015). Conjugate rifted margins width and asymmetry: The interplay between lithospheric strength and thermomechanical processes. *Journal of Geophysical Research: Solid Earth*, *120*, 8672–8700. https://doi.org/10.1002/2015JB012074

Swift, B. A., Sawyer, D., Grow, J., & Klitgord, K. D. (1987). Subsidence, crustal structure, and thermal evolution of Georges Bank basin. *AAPG Bulletin*, *71*(6), 702–718. https://doi.org/10.1306/94887893-1704-11d7-8645000102c1865d

Talwani, M., & Abreu, V. (2000). Inferences regarding initiation of oceanic crust formation from the US East Coast margin and conjugate South Atlantic margins. In W. Mohriak & M. Talwani (Eds.), *Atlantic Rifts and Continental Margins* (Vol. 115, pp. 211–234). Washington, DC: American Geophysical Union.

Talwani, M., Ewing, J., Sheridan, R. E., Holbrook, W. S., & Glover, L. (1995). the EDGE experiment and the US East Coast magnetic anomaly. In *Rifted Ocean-continent boundaries* (pp. 155–181). Dordrecht: Springer.

Taylor, B., Goodliffe, A., & Martinez, F. (2009). Initiation of transform faults at rifted continental margins. *Comptes Rendus Geoscience*, *341*(5), 428–438. https://doi.org/10.1016/j.crte.2008.08.010

Taylor, D., & Anderson, R. (1982). Geophysical studies of the COST Nos. G-1 and G-2 wells. In *Geological Studies of the COST Nos. G-1 and G-2 Wells, United States North Atlantic Outer Continental Shelf* (Vol. 861, pp. 153–188). Reston, VA: United States Geological Survey Circular.

Tetreault, J., & Buiter, S. (2018). The influence of extension rate and crustal rheology on the evolution of passive margins from rifting to break-up. *Tectonophysics*, *746*, 155–172. https://doi.org/10.1016/j.tecto.2017.08.029

Thomas, W. A. (2006). Tectonic inheritance at a continental margin. *GSA Today*, *16*(2), 4–11. https://doi.org/10.1130/1052-5173(2006)016[4:tiaacm]2.0.co;2

Tian, X., & Buck, W. R. (2019). Lithospheric thickness of volcanic rifting margins: Constraints from seaward dipping reflectors. *Journal of Geophysical Research: Solid Earth*, *124*, 3254–3270. https://doi.org/10.1029/2018JB016733

Tréhu, A. M., Ballard, A., Dorman, L., Gettrust, J., Klitgord, K. D., & Schreiner, A. (1989). Structure of the lower crust beneath the Carolina trough, US Atlantic continental margin. *Journal of Geophysical Research*, *94*(B8), 10,585–10,600. https://doi.org/10.1029/JB094ib08p10585

Triezenberg, P., Hart, P., & Childs, J. (2016). National archive of marine seismic surveys (NAMSS)—A USGS data website of marine seismic reflection data within the US exclusive economic zone (EEZ), doi. org/10.5066/F7930R7P.

Vail, P., Todd, R., & Sangree, J. (1977). Seismic stratigraphy and global changes of sea level: Part 5. Chronostratigraphic significance of seismic reflections: Section 2. Application of seismic reflection configuration to stratigraphic interpretation.

van Staal, C. R., Whalen, J. B., Valverde-Vaquero, P., Zagorevski, A., & Rogers, N. (2009). Pre-carboniferous, episodic accretion-related, orogenesis along the Laurentian margin of the northern Appalachians. *Geological Society of London, Special Publication*, *327*(1), 271–316. https://doi.org/10.1144/sp327.13

Van Wijk, J., Huismans, R., Ter Voorde, M., & Cloetingh, S. (2001). Melt generation at volcanic continental margins: No need for a mantle plume? *Geophysical Research Letters*, *28*(20), 3995–3998. https://doi.org/10.1029/2000gl012848

Villeneuve, M. (2005). Paleozoic basins in West Africa and the Mauritanide thrust belt. *Journal of African Earth Sciences*, *43*(1–3), 166–195. https://doi.org/10.1016/j.jafrearsci.2005.07.012

Walker, J., Geissman, J., Bowring, S., & Babcock, L. (2018). Geologic time scale v. 5.0: Geological society of America

Watts, A. (1982). Tectonic subsidence, flexure and global changes of sea level. *Nature*, *297*(5866), 469. https://doi.org/10.1038/297469a0

Wernicke, B. (1985). Uniform-sense normal simple shear of the continental lithosphere. *Canadian Journal of Earth Sciences*, *22*(1), 108–125. https://doi.org/10.1139/e85-009

Wernicke, B., & Tilke, P. (1989). Extensional Tectonic Framework of the U.S. Central Atlantic Passive Margin: Chapter 2: Concepts. *AAPG Memoir*, *46*, 7–21.

Whalen, L., Gazel, E., Vidito, C., Puffer, J., Bizimis, M., Henika, W., & Caddick, M. J. (2015). Supercontinental inheritance and its influence on supercontinental breakup: The central Atlantic magmatic province and the breakup of Pangea. *Geochemistry, Geophysics, Geosystems*, *16*, 3532–3554. https://doi.org/10.1002/2015gc005885

White, C. E., Barr, S. M., & Tollo, R. (2010). Lithochemistry of the lower Paleozoic Goldenville and Halifax groups, southwestern Nova Scotia, Canada: Implications for stratigraphy, provenance, and tectonic setting of Meguma. In R. P. Tollo, M. J. Bartholomew, J. P. Hibbard, P. M. Karabinos (Eds.), *From Rodinia to Pangea: The Lithotectonic record of the Appalachian region* (Vol. 206, pp. 347–366). Boulder, CO: Geological society of America.

White, R. S., & McKenzie, D. (1989). Magmatism at rift zones: The generation of volcanic continental margins and flood basalts. *Journal of Geophysical Research*, *94*(B6), 7685–7729. https://doi.org/10.1029/JB094ib06p07685

White, R. S., Spence, G. D., Fowler, S. R., McKenzie, D. P., Westbrook, G. K., & Bowen, A. N. (1987). Magmatism at rifted continental margins. *Nature*, *330*(6147), 439. https://doi.org/10.1038/330439a0

Whiteside, J. H., Olsen, P. E., Kent, D. V., Fowell, S. J., & Et-Touhami, M. (2007). Synchrony between the Central Atlantic magmatic province and the Triassic–Jurassic mass-extinction event? *Palaeogeography, Palaeoclimatology, Palaeoecology*, *244*(1–4), 345–367. https://doi.org/10.1016/j.palaeo.2006.06.035

Wilson, M. (1997). Thermal evolution of the Central Atlantic passive margins: Continental break-up above a Mesozoic super-plume. *Journal of the Geological Society*, *154*(3), 491–495. https://doi.org/10.1144/gsjgs.154.3.0491

Withjack, M. O., Schlische, R. W., & Olsen, P. E. (1998). Diachronous rifting, drifting, and inversion on the passive margin of central eastern North America: An analog for other passive margins. *AAPG Bulletin*, *82*(5), 817–835. https://doi.org/10.1306/1d9bc60b-172d-11d7-8645000102c1865d

Withjack, M. O., Schlische, R. W., & Olsen, P. E. (2002). Rift-basin structure and its influence on sedimentary systems.

Withjack, M. O., Schlische, R. W., & Olsen, P. E. (2012). Development of the passive margin of eastern North America: Mesozoic rifting, Igneous activity, and breakup.

Wolfenden, E., Ebinger, C., Yirgu, G., Renne, P. R., & Kelley, S. P. (2005). Evolution of a volcanic rifted margin: Southern Red Sea, Ethiopia. *Geological Society of America Bulletin*, *117*(7–8), 846–864. https://doi.org/10.1130/b25516.1

Wu, Y., Louden, K. E., Funck, T., Jackson, H. R., & Dehler, S. A. (2006). Crustal structure of the Central Nova Scotia margin off eastern Canada. *Geophysical Journal International*, *166*(2), 878–906. https://doi.org/10.1111/j.1365-246x.2006.02991.x

Wyer, P., & Watts, A. (2006). Gravity anomalies and segmentation at the East Coast, USA continental margin. *Geophysical Journal International*, *166*(3), 1015–1038. https://doi.org/10.1111/j.1365-246x.2006.03066.x

Ziegler, P. A., & Cloetingh, S. (2004). Dynamic processes controlling evolution of rifted basins. *Earth-Science Reviews*, *64*(1–2), 1–50. https://doi.org/10.1016/s0012-8252(03)00041-2

References From the Supporting Information

Adinolfi, F. (1986). Murphy Wilmington Canyon 106-1 Well, US Miner. Manage. Serv. Outer Cont. Shelf Rep. MMS, 86-0117.

Amato, R. V. (1987). Shell Baltimore Rise 93-1 Well, US Miner. Manage. Serv. Outer Cont. Shelf Rep. MMS, 86-0128.

Amato, R. V., & Bielak, L. (1990). Texaco Hudson Canyon 642-1 Well, Minerals Management Service OCS Report MMS, 89-0027.

Bielak, L. (1986). Tenneco Hudson Canyon 642-2 well, geological & operational summary rep, 29 pp.

Bifano, F. V. (1978). Gulf energy and minerals block 857, Hudson Canyon, #1 OCS A-0059, Baltimore Canyon area. Report for well API #61-105-00008, Paleo-Data, Inc.Rep

Cousminer, H. L., Steinkraus, W., & Hall, R. (1986). Paleontology: Exxon OCS-A 0029-1, block 599-1. Report for well API #61-105-00019. Rep

Crane, M. J. (1979a). Exxon block 684-1 Hudson Canyon paleontological summary Rep, Exxon Production Research Company.

Crane, M. J. (1979b). Exxon block 684-2 Hudson Canyon paleontological summary rep, Exxon Production Research Company.

Crane, M. J. (1979c). Geologic summary exxon OCS-A-0009 No. 1 North Mallard, paleontological section Rep, Exxon.

Crane, M. J. (1979d). Geologic summary exxon OCS-A-0065 #1 Canvasback rep, Exxon Production Research Company.

Crane, M. J. (1981). Exxon block 816-1 paleontological summary Rep, Exxon Production Research Company.

Edelman, D. W., Gauger, D. J., Percival, S. F., & Thompson, L. B. (1979). Biostratigraphy, paleoecology, visual kerogen analysis, vitrinite reflectance studies, and hydrocarbon source-bed evaluation of the Mobil 17-2 well, Avalon area, offshore New Jersey. Report for well API #61-104-00005 Rep.

Edson, G. M. (1986). Shell Wilmington Canyon 586-1 well, geological and operational summary.

Edson, G. M. (1987a). Shell Wilmington Canyon 372-1 Well.

Edson, G. M. (1987b). Shell Wilmington Canyon 587-1 well, geological and operational summary: Minerals management service OCS report MMS 87-0074 rep, 49 pp.

Edson, G. M., Olson, D. L., & Petty, A. J. (2000a). Exxon Lydonia Canyon Block 133 No. 1 Well, U. S. Department of the interior OCS report, MMS 2000–033, 52.

Edson, G. M., Olson, D. L., & Petty, A. J. (2000b). Mobil Lydonia Canyon Block 273 No. 1 Well, U. S. Department of the interior OCS report, MMS 2000-036.

Edson, G. M., Olson, D. L., & Petty, A. J. (2000c). Shell Lydonia Canyon Block 357 No. 1 Well, U. S. Department of the interior OCS report, MMS 2000-038.

Edson, G. M., Olson, D. L., & Petty, A. J. (2000d). Tenneco Lydonia Canyon Block 187 No. 1 Well, U. S. Department of the interior OCS report, MMS 2000-035

Gauger, D. J., Griffith, C. E., Percival, S. F., & Thompson, L. B. (1979). Biostratigraphy, paleoecology, kerogen/tai analysis, vitrinite reflectance and geochemical analysis of the mobil 544—La Well, Baltimore Canyon, Offshore New Jersey Rep, Mobil Stratigraphic Laboratory.

International Biostratigraphers Incorporated (1978a). Biostratigraphy of the continental Oil OCS-A-Oo24 Blk. 590 Hudson Canyon well #1 rep, 13 pp.

International Biostratigraphers Incorporated (1978b). Biostratigraphy of the Houston oil 8. Minerals OCS-A-Uliz block 675 No. L well rep, 12 pp.

International Biostratigraphers Incorporated (1979a). Biostratigraphy of the Houston Oil 8. Minerals OCS-A-0057 block 855 No. L well rep, 11 pp.

International Biostratigraphers Incorporated (1979b). Biostratigraphy of the Tenneco OCS A-0131 block 495 N0.1 well rep.

Kobelski, B. J. (1987). Texaco Hudson Canyon in 598-3 well rep, 30 pp.

Picou, J. E. B. (1978). Shell 632–1 paleontological investigation summary rep.

Poppe, L., Hall, R., Cousminer, H., Stanton, R., & Steinkraus, W. (1990). Biostratigraphy, lithofacies and paleoenvironments of the Gulf 718-1 well, US mid-Atlantic outer continental shelf. *Marine Geology*, *92*(1–2), 27–50. https://doi.org/10.1016/0025-3227(90)90025-f

Poppe, L., & Poag, C. (1993). Mesozoic stratigraphy and paleoenvironments of the Georges Bank Basin: A correlation of exploratory and COST wells. *Marine Geology*, *113*(3–4), 147–162. https://doi.org/10.1016/0025-3227(93)90015-n

Siegel, J., Dugan, B., Lizarralde, D., Person, M., DeFoor, W., & Miller, N. (2012). Geophysical evidence of a late Pleistocene glaciation and paleo-ice stream on the Atlantic continental shelf offshore Massachusetts, USA. *Marine Geology*, *303*, 63–74. https://doi.org/10.1016/j.margeo.2012.01.007

Steinkraus, W. E. (1979). Paleontological summary and biostratigraphic report. Report for Well API #61–104-00001, Shell Oil Company, Southeastern Region, Offshore Exploration Division. Rep

Stough, J. B. (1981). Palynology of the Exxon OCS-a-Oo52 no. 1, block 728, south pintail Prospect, offshore New Jersey (Hudson canyon) rep, Exxon company, U.S.A.